Chapter 2
Fundamental Theories and Analytical Methods for Vibrations of Simply-Supported Beams Under Moving Loads

In this chapter, some fundamental theories and methods for vibration analysis of simply-supported beams under moving loads are presented. The analytical solutions of vibrations induced by a moving concentrated load, a moving harmonic load, and a moving wheel-spring-mass (WSM) load with varying speed are deduced, respectively, and the vibration characteristics of them are investigated in several case studies. In addition, as one of the important phenomena related to the train-bridge coupling vibration, the mechanisms of vibration resonance, suppression, and cancellation happened in the moving load and beam system are analyzed.

2.1 Vibrations of Simply-Supported Beam Under Moving Loads

2.1.1 Analysis Model

For a simply-supported beam subjected to a moving load, if the mass of the load is much smaller than that of the beam, the inertial force caused by the mass of the load can be neglected, and the load becomes a moving concentrated force varying with time, denoted as $P(t)$. In this case, a simplified analysis model is established, as shown in Fig. 2.1.

Assuming the simply-supported beam has a uniform cross section with constant bending stiffness EI, a uniformly distributed mass $\bar{m}$ per unit length, a viscous damping with the damping force proportional to the vibration velocity, and the small and elastic deformation during its vibration excited by a moving concentrated load $P(t)$ with the constant speed V, as shown in the coordinates shown in Fig. 2.1, the motion equation for the beam subjected to the moving concentrated load can be expressed as

H. Xia et al., *Dynamic Interaction of Train-Bridge Systems in High-Speed Railways*, Advances in High-speed Rail Technology, https://doi.org/10.1007/978-3-662-54871-4_2

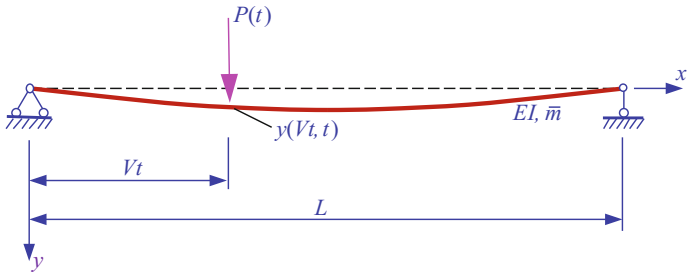

Fig. 2.1 Simply-supported beam under a moving concentrated load

$$EI\frac{\partial^4 y(x,t)}{\partial x^4}+\bar{m}\frac{\partial^2 y(x,t)}{\partial t^2}+c\frac{\partial y(x,t)}{\partial t}=\delta(x-Vt)P(t) \tag{2.1}$$

where c is the damping coefficient of the beam; δ is the Dirac function, a useful function for this analysis, which has the following characteristics

$$\delta(x-\eta)=\begin{cases}\infty, & (x=\eta)\\ 0, & (x\neq\eta)\end{cases} \tag{2.2a}$$

$$\int_{-\infty}^{\infty}\delta(x-\eta)f(x)\mathrm{d}x=f(\eta) \tag{2.2b}$$

$$\int_{a}^{b}\delta(x-\eta)f(x)\mathrm{d}x=\begin{cases}0, & (\eta<a<b)\\ f(\eta), & (a\leq\eta\leq b)\\ 0, & (a<b<\eta)\end{cases} \tag{2.2c}$$

Equation (2.1) is a partial differential equation. It can be solved by the modal decomposition method, namely the separation of variables in mathematics. In this method, the geometric coordinates of the structure are transformed into the modal coordinates or the generalized coordinates. Accordingly, the motion of the structure can be represented by the superposition of modal movements (Clough and Penzien 2003). For a one-dimensional continuous structure, the transformation can be described by

$$y(x,t)=\sum_{i=1}^{\infty}\phi_i(x)\cdot q_i(t) \tag{2.3}$$

where $q_i(t)$ is the generalized coordinate varying with time t, and $\phi_i(x)$ is the modal function. Equation (2.3) shows that any rational displacement of the structure can be expressed by superposition of the corresponding amplitudes of all the modes.

The modal component of any deformation of the structure can be acquired by using the orthogonality of the modes. For a beam with uniform section, the contribution of the nth mode to the displacement $y(x, t)$ can be obtained by multiplying $\phi_n(x)$ on both sides of Eq. (2.3) and integrating them along the axle of the beam as

$$\int_0^L \phi_n(x) y(x,t) \mathrm{d}x = \sum_{i=1}^{\infty} q_i(t) \int_0^L \phi_n(x) \phi_i(x) \mathrm{d}x \tag{2.4}$$

Due to the orthogonality of modes, the right-hand side of Eq. (2.3) equals to zero when $i \neq n$, and only one term of the infinite series is left. Consequently, the generalized coordinates of the nth mode can be expressed as

$$q_n(t) = \frac{\int_0^L \phi_n(x) y(x,t) \mathrm{d}x}{\int_0^L \phi_n^2(x) \mathrm{d}x} \tag{2.5}$$

By decomposing the motion equation of the simply-supported beam based on the above principle, and substituting Eq. (2.3) into Eq. (2.1), we obtain

$$EI \sum_{i=1}^{\infty} q_i(t) \frac{\mathrm{d}^4 \phi_i(x)}{\mathrm{d}x^4} + \bar{m} \sum_{i=1}^{\infty} \phi_i(x) \frac{\mathrm{d}^2 q_i(t)}{\mathrm{d}t^2} + c \sum_{i=1}^{\infty} \phi_i(x) \frac{\mathrm{d}q_i(t)}{\mathrm{d}t} = \delta(x - Vt) P(t) \tag{2.6}$$

By multiplying each term of Eq. (2.6) with the nth modal function $\phi_n(x)$, conducting integration along the length of the beam, and considering the orthogonality of modes, the motion equation in generalized coordinate corresponding to the nth mode is given by

$$\begin{aligned} EIq_n(t) \int_0^L \phi_n(x) \frac{\mathrm{d}^4 \phi_n(x)}{\mathrm{d}x^4} \mathrm{d}x + \bar{m} \frac{\mathrm{d}^2 q_n(t)}{\mathrm{d}t^2} \int_0^L \phi_n^2(x) \mathrm{d}x + c \frac{\mathrm{d}q_n(t)}{\mathrm{d}t} \int_0^L \phi_n^2(x) \mathrm{d}x \\ = \int_0^L \delta(x - Vt) P(t) \phi_n(x) \mathrm{d}x \end{aligned} \tag{2.7}$$

For the simply-supported beam with uniform section, the modal function can be assumed as a trigonometric function

$$\phi_n(x) = \sin \frac{n\pi x}{L} \tag{2.8}$$

Substituting it into Eq. (2.7), and noting the following formulas

$$\int_0^L \sin^2 \frac{n\pi x}{L} \mathrm{d}x = \frac{L}{2}$$
$$\int_0^L \delta(x - Vt) P(t) \sin \frac{n\pi x}{L} \mathrm{d}x = P(t) \sin \frac{n\pi Vt}{L}$$

The following motion equation can be obtained

$$\frac{L}{2}\bar{m}\frac{\mathrm{d}^2 q_n(t)}{\mathrm{d}t^2} + \frac{L}{2}c\frac{\mathrm{d}q_n(t)}{\mathrm{d}t} + \frac{L}{2}\frac{n^4\pi^4}{L^4}EIq_n(t) = P(t)\sin\frac{n\pi Vt}{L} \tag{2.9}$$

For the simply-supported beam with uniform section, the nth circular frequency and the nth damping coefficient are $\omega_n = \frac{n^2\pi^2}{L^2}\sqrt{\frac{EI}{\bar{m}}}$ and $c_n = 2\xi_n\bar{m}\omega_n$, respectively. Dividing both sides of Eq. (2.9) by $\frac{\bar{m}L}{2}$ and introducing $\dot{q} = \frac{\mathrm{d}q}{\mathrm{d}t}$ and $\ddot{q} = \frac{\mathrm{d}^2 q}{\mathrm{d}t^2}$, the standard form of the nth modal equation for the simply-supported beam under moving load can be written as

$$\ddot{q}_n(t) + 2\xi_n\omega_n\dot{q}_n(t) + \omega_n^2 q_n(t) = \frac{2}{\bar{m}L}P(t)\sin\frac{n\pi Vt}{L} \tag{2.10}$$

For convenience of discussion, two parameters are introduced herein, the critically damped circular frequency $\omega_b = c/2\bar{m} = \xi_n\omega_n$ (Frýba 1999) and the circular frequency $\bar{\omega} = \pi V/L$ of excitation (Xia et al. 2006). Accordingly, Eq. (2.10) can be rewritten as

$$\ddot{q}_n(t) + 2\omega_\mathrm{b}\dot{q}_n(t) + \omega_n^2 q_n(t) = \frac{2}{\bar{m}L}P(t)\sin n\bar{\omega}t \tag{2.11}$$

Equation (2.11) is a linear differential equation with constant coefficients, and obviously, the equations for different modes are independent. By using the Duhamel integral, the particular solution can be obtained as

$$q_n(t) = \frac{2}{\bar{m}L\omega_\mathrm{D}^n}\int_0^t P(\tau)\sin n\bar{\omega}\tau \mathrm{e}^{-\omega_\mathrm{b}(t-\tau)}\sin\omega_\mathrm{D}^n(t-\tau)\mathrm{d}\tau \tag{2.12}$$

where $\omega_\mathrm{D}^n = \omega_n\sqrt{1-\xi_n^2}$ is the nth natural frequency of the damped structure. Equation (2.12) is suited for structures in undercritically damped and critically damped cases.

For a simple load, such as a moving constant load $P(t) = P$ or a moving harmonic load $P(t) = P\sin\omega t$, the closed-form solution of Eq. (2.12) can be obtained by integration. In the following sections, the analytical solutions for the simply-supported beam under the above two types of simple loads are deduced, with emphasis on the discussion of several special cases related to the moving constant load.

2.1.2 Vibration of Simply-Supported Beam Under a Moving Concentrated Load

In the case of a moving constant load, i.e., $P(\tau) = P$, Eq. (2.12) can be expressed as

$$q_n(t) = \frac{2P}{\bar{m}L\omega_{\mathrm{D}}^n}\int_0^t \sin n\bar{\omega}\tau \, \sin\omega_{\mathrm{D}}^n(t-\tau)\mathrm{e}^{-\omega_{\mathrm{b}}(t-\tau)}\mathrm{d}\tau \tag{2.13}$$

By using the following triangular transformation formula (Rade and Westergren 2010)

$$\sin n\bar{\omega}\tau \, \sin\omega_{\mathrm{D}}^n(t-\tau) = \frac{1}{2}\left\{\cos[\omega_{\mathrm{D}}^n t - (\omega_{\mathrm{D}}^n + n\bar{\omega})\tau] - \cos[\omega_{\mathrm{D}}^n t - (\omega_{\mathrm{D}}^n - n\bar{\omega})\tau]\right\} \tag{2.14}$$

and the exact solutions of the following two integrations

$$\int_0^t \sin(a+b\tau)\mathrm{e}^{(c+d\tau)}\mathrm{d}\tau = \frac{1}{b^2+d^2}\left\{[d\,\sin(a+b\tau) - b\,\cos(a+b\tau)]\mathrm{e}^{(c+d\tau)}\right\}\Big|_0^t \tag{2.15a}$$

$$\int_0^t \cos(a+b\tau)\mathrm{e}^{(c+d\tau)}\mathrm{d}\tau = \frac{1}{b^2+d^2}\left\{[b\,\sin(a+b\tau) + d\,\cos(a+b\tau)]\mathrm{e}^{(c+d\tau)}\right\}\Big|_0^t \tag{2.15b}$$

and substituting Eq. (2.14) into Eq. (2.13), and by utilizing Eq. (2.15a, 2.15b), the solution of Eq. (2.13) can be obtained as

$$\begin{aligned} q_n(t) &= \frac{P}{\bar{m}L\omega_{\mathrm{D}}^n}\left\{\int_0^t \cos[\omega_{\mathrm{D}}^n t - (\omega_{\mathrm{D}}^n + n\bar{\omega})\tau]\,\mathrm{e}^{-\omega_{\mathrm{b}}(t-\tau)}\mathrm{d}\tau\right. \\ &\quad \left. - \int_0^t \cos[\omega_{\mathrm{D}}^n t - (\omega_{\mathrm{D}}^n - n\bar{\omega})\tau]\mathrm{e}^{-\omega_{\mathrm{b}}(t-\tau)}\mathrm{d}\tau\right\} \\ &= \frac{P}{\bar{m}L\omega_{\mathrm{D}}^n}\left\{\frac{1}{(\omega_{\mathrm{D}}^n + n\bar{\omega})^2 + \omega_{\mathrm{b}}^2}\left\{[(\omega_{\mathrm{D}}^n + n\bar{\omega})\sin n\omega t + \omega_{\mathrm{b}}\cos n\bar{\omega}t]\right.\right. \\ &\quad \left.\left. + [(\omega_{\mathrm{D}}^n + n\bar{\omega})\sin\omega_{\mathrm{D}}^n t - \omega_{\mathrm{b}}\cos\omega_{\mathrm{D}}^n t]\mathrm{e}^{-\omega_{\mathrm{b}}t}\right\}\right. \\ &\quad \left. - \frac{1}{(\omega_{\mathrm{D}}^n - n\bar{\omega})^2 + \omega_{\mathrm{b}}^2}\left\{[-(\omega_{\mathrm{D}}^n - n\bar{\omega})\sin n\omega t + \omega_{\mathrm{b}}\cos n\bar{\omega}t]\right.\right. \\ &\quad \left.\left. + [(\omega_{\mathrm{D}}^n - n\bar{\omega})\sin\omega_{\mathrm{D}}^n t - \omega_{\mathrm{b}}\cos\omega_{\mathrm{D}}^n t]\mathrm{e}^{-\omega_{\mathrm{b}}t}\right\}\right\} \end{aligned} \tag{2.16}$$

Note that $\omega_{\mathrm{D}}^{n2} = \omega_n^2 - \omega_{\mathrm{b}}^2$ and $\omega_{\mathrm{D}}^{n2} = 0$ are, respectively, valid in the undercritically damped case and the critically damped case, and Eq. (2.16) is rewritten separately for the two cases as

$$q_n(t) = \frac{2P}{\bar{m}L}\frac{1}{(\omega_n^2 - n^2\bar{\omega}^2)^2 + 4\omega_{\mathrm{b}}^2 n^2\bar{\omega}^2}\Big\{(\omega_n^2 - n^2\bar{\omega}^2)\sin n\bar{\omega}t - \frac{n\omega[(\omega_n^2 - n^2\bar{\omega}^2) - 2\omega_{\mathrm{b}}^2]}{(\omega_n^2 - \omega_{\mathrm{b}}^2)^{1/2}}\mathrm{e}^{-\omega_{\mathrm{b}}t}\sin\omega_{\mathrm{D}}^n t - 2\omega_{\mathrm{b}} n\bar{\omega}(\cos n\bar{\omega}t - \mathrm{e}^{-\omega_{\mathrm{b}}t}\cos\omega_{\mathrm{D}}^n t)\Big\} \tag{2.17a}$$

$$q_n(t) = \frac{2P}{\bar{m}L}\frac{1}{(\omega_n^2 + n^2\bar{\omega}^2)^2}\Big\{(\omega_n^2 - n^2\bar{\omega}^2)\sin n\omega t - 2\omega_n n\bar{\omega}\cos n\bar{\omega}t + \mathrm{e}^{-\omega_{\mathrm{b}}t}[(\omega_n^2 + n^2\bar{\omega}^2)n\bar{\omega}t + 2\omega_n n\bar{\omega}]\Big\} \tag{2.17b}$$

For convenience of discussing the influences of load moving speed and structural damping on the vibration responses of the bridge, two dimensionless parameters, i.e., speed parameter α and damping parameter μ, are introduced, which are defined by

$$\alpha = \frac{\bar{\omega}}{\omega_1} = \frac{VL}{\pi}\left(\frac{\bar{m}}{EI}\right)^{1/2} = \frac{V}{V_{\mathrm{cr}}} \tag{2.18a}$$

$$\mu = \frac{\omega_{\mathrm{b}}}{\omega_1} = \frac{\omega_{\mathrm{b}}L^2}{\pi}\left(\frac{\bar{m}}{EI}\right)^{1/2} \tag{2.18b}$$

where $V_{\mathrm{cr}} = \frac{2f_n L}{n^2} = \frac{\pi}{L}\left(\frac{EI}{\bar{m}}\right)^{1/2}$ (n = 1, 2, 3, …) means the critical speed, f_n is the nth natural frequency of the beam, and EI is the bending stiffness of the bridge. When the load moving speed is n times of the critical speed, the resonance of the nth mode will be induced. More details can be found in Sect. 2.3.

By introducing Eq. (2.18a, 2.18b), Eq. (2.17a, 2.17b) becomes

$$q_n(t) = y_0\frac{1}{n^2[n^2(n^2 - \alpha^2)^2 + 4\alpha^2\mu^2]}\Big\{n^2(n^2 - \alpha^2)\sin n\bar{\omega}t - \frac{n\alpha[n^2(n^2 - \alpha^2) - 2\mu^2]}{(n^4 - \mu^2)^{1/2}}\mathrm{e}^{-\omega_{\mathrm{b}}t}\sin\omega_{\mathrm{D}}^n t - 2n\alpha\mu(\cos n\bar{\omega}t - \mathrm{e}^{-\omega_{\mathrm{b}}t}\cos\omega_{\mathrm{D}}^n t)\Big\} \tag{2.19a}$$

$$q_n(t) = y_0\frac{1}{n^2(n^2 + \alpha^2)^2}\Big\{(n^2 - \alpha^2)\sin n\bar{\omega}t - 2n\alpha\cos n\bar{\omega}t + \mathrm{e}^{-\omega_n t}[(n^2 + \alpha^2)n\bar{\omega}t + 2n\alpha]\Big\} \tag{2.19b}$$

where $y_0 = \frac{PL^3}{48EI} \approx \frac{2PL^3}{\pi^4 EI} = \frac{2P}{\bar{m}L\omega_1^2}$, indicating the displacement of the bridge at mid-span where a concentrated force P is applied.

By the modal decomposition method, the particular solution to the displacement response of the simply-supported beam in undercritically damped case can be expressed as

$$y(x,t) = y_0 \sum_{n=1}^{\infty} \frac{1}{n^2[n^2(n^2-\alpha^2)^2 + 4\alpha^2\mu^2]} \{n^2(n^2-\alpha^2)\sin n\bar{\omega}t - \frac{n\alpha[n^2(n^2-\alpha^2)-2\mu^2]}{(n^4-\mu^2)^{1/2}} e^{-\omega_b t}\sin\omega_D^n t - 2n\alpha\mu(\cos n\bar{\omega}t - e^{-\omega_b t}\cos\omega_D^n t)\} \sin\frac{n\pi x}{L} \tag{2.20}$$

in which $q_n(t)$ is the generalized coordinate of the nth mode given by Eq. (2.19a, 2.19b).

Based on Eq. (2.20), several special cases are discussed hereinbelow.

2.1.2.1 Static Load Case ($\alpha = 0$)

When the speed parameter $\alpha = 0$, Eq. (2.20) becomes

$$y(x,t) = y_0 \sum_{n=1}^{\infty} \frac{1}{n^4} \sin\frac{n\pi x}{L} \sin n\bar{\omega}t = y_0 \sum_{n=1}^{\infty} \frac{1}{n^4} \sin\frac{n\pi x}{L} \sin\frac{n\pi Vt}{L} \tag{2.21}$$

In this case, the problem becomes the solution of the bridge displacement at position x when a static load P acts at position Vt. Herein, Vt indicates the moving distance of the load on the bridge. Equation (2.21) can be regarded as the Fourier expansion of the influence line of bridge displacement at position x, or the Fourier expansion of the bridge deflection curve when a concentrated load P acts at the position Vt.

2.1.2.2 Undamped Case ($\mu = 0$)

(1) $\alpha \neq k$, $\mu = 0$

As will be demonstrated later, when the speed parameter of the load meets $\alpha = k$, the resonance with the nth mode can be caused. Hence, the load speed corresponding to $\alpha = k$ is called as the resonant speed.

First, consider the case where the load moves on the bridge at non-resonance speed, i.e., $\alpha \neq k$.

In the undamped case $\mu = 0$, Eq. (2.20) becomes

$$y(x,t) = y_0 \sum_{n=1}^{\infty} \sin\frac{n\pi x}{L} \frac{1}{n^2(n^2-\alpha^2)} \left(\sin n\bar{\omega}t - \frac{\alpha}{n}\sin\omega_n t\right) \tag{2.22}$$

According to this equation, the first-order mode contributes most to the displacement, which means high precision can be reached by using the first-order vibration mode when solving the bridge displacement under dynamic loads.

Considering the terms within the parentheses of Eq. (2.22), and letting them equal to zero at the time when the load is about to leave the bridge, namely at $t = L/V$, the following equation is obtained

$$\left(\sin n\bar{\omega}t - \frac{\alpha}{n}\sin\omega_n t\right)\Big|_{t=\frac{L}{V}} = \sin n\pi - \frac{\alpha}{n}\sin\frac{n^2\pi}{\alpha} = 0 \tag{2.23}$$

It is easy to see when $\alpha = n^2/k$ ($k = 1, 2, 3, \ldots, k \neq n$), Eq. (2.23) is valid. Assuming $\alpha = n^2/k$ corresponds to a speed V_{can}, we have

$$\alpha = \frac{V_{can}}{V_{cr}} \Rightarrow V_{can} = \alpha V_{cr} \tag{2.24}$$

By substituting Eq. (2.18a) into Eq. (2.24), and using the theoretical frequency of the simply-supported beam $f_1 = f_n/n^2$, V_{can} can be expressed as

$$V_{can} = \alpha V_{cr} = \frac{n^2}{k} \cdot \frac{2f_n L}{n^2} = 2n^2 f_1 L/k \tag{2.25}$$

Equations (2.22) and (2.23) show that when $\alpha = n^2/k$, the bridge displacement component of the nth vibration mode becomes null at the time $t = L/V$, and thus, V_{can} is called the cancellation speed corresponding to the nth vibration mode of the beam.

When the load moves out of the bridge, i.e., when $t > L/V$, the beam is in free vibration. The displacement solution of the bridge will be

$$y(x,t) = \sum_{n=1}^{\infty} \left[\frac{\dot{y}_n(x, L/V)}{\omega_n}\sin\omega_n t + y_n(x, L/V)\cos\omega_n t\right] \tag{2.26}$$

where $y_n(x, L/V)$ and $\dot{y}_n(x, L/V)$ are, respectively, displacement and velocity of the bridge at $t = L/V$, which can be expressed as

$$y_n(x, L/V) = \frac{y_0}{n^2(n^2-\alpha^2)} \left(\sin\frac{n\bar{\omega}L}{V} - \frac{\alpha}{n}\sin\frac{\omega_n L}{V}\right) \sin\frac{n\pi x}{L} \tag{2.27a}$$

$$\dot{y}_n(x, L/V) = \frac{n\bar{\omega}y_0}{n^2(n^2-\alpha^2)}\left(\cos\frac{n\bar{\omega}L}{V} - \cos\frac{\omega_n L}{V}\right)\sin\frac{n\pi x}{L} \tag{2.27b}$$

At the moment when the load moves out of the bridge at the cancellation speed V_{can}, the vibration velocity of the bridge is not necessarily equal to zero, while it can be expressed as

$$\begin{aligned}\dot{y}(x,t)|_{t=\frac{L}{V}} &= \left(V\frac{\partial y(x,t)}{\partial x} + \frac{\partial y(x,t)}{\partial t}\right)\Bigg|_{t=L/V} \\ &= y_0\sum_{n=1}^{\infty}\sin\frac{n\pi x}{L}\frac{n\bar{\omega}}{n^2(n^2-\alpha^2)}(\cos n\pi - \cos k\pi)\end{aligned} \tag{2.28}$$

It can be observed from Eq. (2.28) that when n and k have the same parity, Eq. (2.26) equals zero, indicating no displacement and velocity exist on the bridge after the load leaves the bridge, namely the bridge becomes motionless. When n and k are with different parity, only the displacement is zero, while the velocity is not, which makes the bridge continue to vibrate, namely as a residual vibration. Correspondingly, V_{can} given in Eq. (2.25) is defined as full cancellation speed in the case with same parity and as the displacement cancellation speed with different parity.

When a series of loads travels at full cancellation speed, the vibration of the bridge will totally disappear after all the loads leave the bridge, due to the linear superposition of all null displacements induced by the loads.

(2) $\alpha = k$, $\mu = 0$

In the case of $\alpha = k$ and $\mu = 0$, Eq. (2.20) becomes an indeterminate form due to 0/0, and its extreme value can be evaluated by applying the L'Hospital's rule. Thus, the particular solution of the bridge displacement can be expressed as

$$\begin{aligned}y(x,t) = {} & y_0\frac{1}{2k^4}(\sin k\bar{\omega}t - k\bar{\omega}t\cos k\bar{\omega}t)\sin\frac{k\pi x}{L} \\ & + y_0\sum_{n=1,n\neq k}^{\infty}\sin\frac{n\pi x}{L}\frac{1}{n^2(n^2-\alpha^2)}\left(\sin n\bar{\omega}t - \frac{\alpha}{n}\sin\omega_n t\right)\end{aligned} \tag{2.29}$$

It is found that when $\alpha = k$ and $\mu = 0$, the bridge displacement at any position x increases with the time t and reaches to the maximum value at $t = L/V$, but not to infinity.

This situation is equivalent to the occurrence of resonance between the bridge and the moving load P. When $k = n$, i.e., $\sin(n\pi Vt/L) = \sin n\bar{\omega}t$, the loading frequency of the moving load coincides with the natural frequency of the nth bridge mode. Moreover, in the case of $k = 1$, the dynamic amplification factor of resonant displacements reaches the maximum, which again indicates that the first mode contributes most to the displacement.

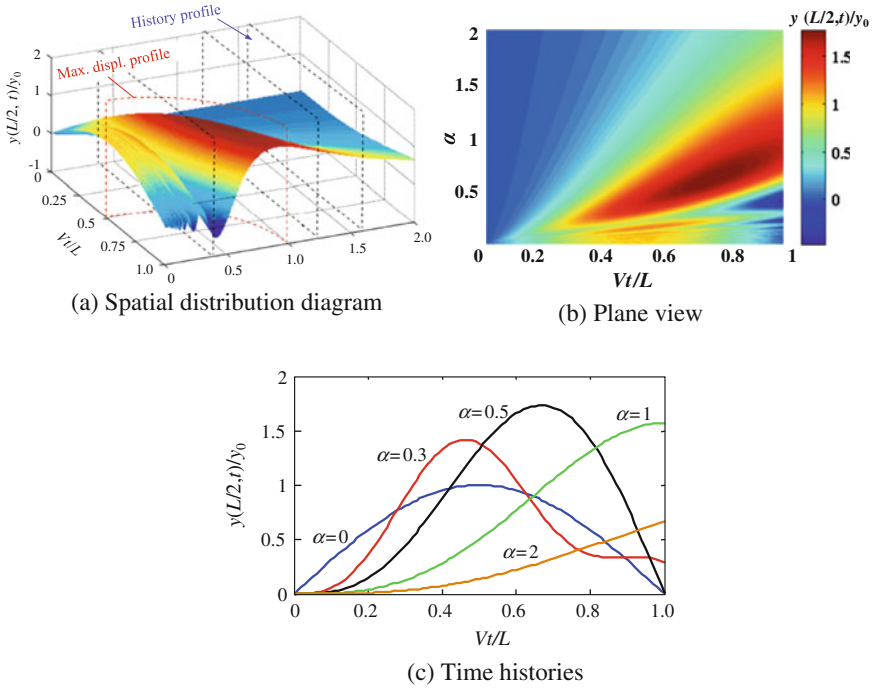

Fig. 2.2 Distributions of mid-span displacement $y(L/2, t)/y_0$ versus time Vt/L and load speed α ($\mu = 0$)

Shown in Fig. 2.2a is the spatial distribution of bridge mid-span displacement subjected to a single moving load, herein expressed with the relative displacement $y(L/2, t)/y_0$ versus time parameter Vt/L and speed parameter α, and in Fig. 2.2b is its plane view. In Fig. 2.2a, the intersecting lines of the curved surfaces with the planar α are the displacement time histories of the bridge, respectively, related to various load speeds of $\alpha = 0$, 0.3, 0.5, 1, 2, as shown in Fig. 2.2c. It is found that at low speed, the maximum mid-span displacement appears when the load is near the bridge center. With the increase of speed, the load position producing the maximum mid-span displacement shifts toward the beam-end, and at certain speed, the mid-span displacement reaches the maximum just at the moment when the load is leaving the bridge.

Shown in Fig. 2.3 is the variation of maximum relative displacement $y_{max}(L/2, t)/y_0$ of the bridge at mid-span versus load speed parameter α. It is found that the maximum displacement does not increase monotonously with the load speed, while some peaks appear at certain speeds, fluctuating in a pattern similar to half sine wave series.

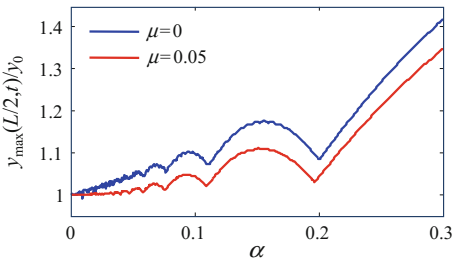

Fig. 2.3 Relation of maximum mid-span displacements with load speed α ($\mu = 0$ and $\mu = 0.05$)

2.1.2.3 Undercritically Damped Case

(1) $\alpha \neq k$, $\mu \ll 1$

When the bridge is undercritically damped, μ and μ^2 in Eq. (2.20) can be neglected, and the following formula similar to Eq. (2.22) can be obtained

$$y(x,t) \approx y_0 \sum_{n=1}^{\infty} \sin\frac{n\pi x}{L} \frac{1}{n^2(n^2-\alpha^2)} \left(\sin n\bar{\omega}t - \frac{\alpha}{n} e^{-\omega_b t} \sin \omega_n t\right) \tag{2.30}$$

Equation (2.30) is very practical in engineering, because the damping of bridges is usually very small, and the driving speed of actual vehicles can never achieve the case of $\alpha = k$ ($V = kV_{cr}$). For example, for the bridge with the span of $L = 32$ m, the first natural frequency $f_1 = 4.5$ Hz, and $k = 1$, the critical speed is calculated as $V_{cr} = 2f_1L = 288$ m/s (1036.8 km/h), which is much higher than the current train speed.

When the train speed is low, there is $\alpha \ll 1$. If the vehicle mass is small compared to the bridge mass, the vehicle can be modeled as a series of moving concentrated loads by ignoring its mass. In this case, the bridge displacement under train loads can be solved by considering only the first-order mode. Thus, the simplified solution of bridge displacement under a single moving load is expressed as

$$y(x,t) \approx y_0 \sin\frac{\pi x}{L} \sin n\bar{\omega}t \tag{2.31}$$

(2) $\alpha = k$, $\mu \ll 1$

The derivation in this case is similar to that when $\alpha = k$, $\mu = 0$, and the bridge displacement is directly given by

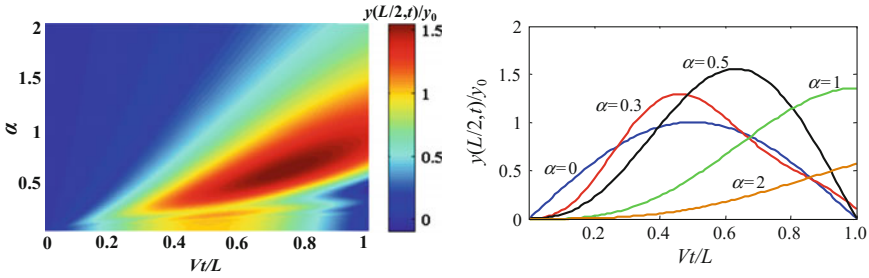

(a) Plane view (b) Time history

Fig. 2.4 Distribution of mid-span displacement $y(L/2, t)/y_0$ versus time Vt/L and velocity α ($\mu = 0.05$)

$$y(x,t) \approx y_0 \frac{1}{2k^4}\left[e^{-\omega_b t}\sin k\bar{\omega}t - \frac{k^2}{\mu}(1-e^{-\omega_b t})\cos k\bar{\omega}t\right]\sin\frac{k\pi x}{L} + y_0\sum_{n=1,n\neq k}^{\infty}\frac{1}{n^2(n^2-\alpha^2)}\left(\sin n\bar{\omega}t - \frac{\alpha}{n}e^{-\omega_b t}\sin\omega_n t\right)\sin\frac{n\pi x}{L} \tag{2.32}$$

Shown in Fig. 2.4a is the plane view of mid-span displacement distribution of the undercritically damped bridge ($\mu = 0.05$) varying with time Vt/L and load speed α, and in Fig. 2.4b are the time history curves of $y(L/2, t)/y_0$ versus Vt/L in various speed parameters. The variation of maximum displacement $y_{max}(L/2, t)/y_0$ versus load speed α is demonstrated in Fig. 2.3. By comparing the curves in the two damping cases, it can be found that the damping effect decreases the bridge displacement, but does not obviously change the variation trend of maximum displacement with speed parameter.

2.1.2.4 Critically Damped Case ($\mu = \mu_{cr} = k^2$)

When the damping ratio ξ_k is equal to 1, the kth mode of the bridge is critically damped, and thus, the critical damping parameter becomes

$$\mu_{cr} = \frac{\omega_b}{\omega_1} = \frac{\xi_k\omega_k}{\omega_1} = k^2 \tag{2.33}$$

In this case, the generalized coordinate $q_k(t)$ of the kth mode of the simply-supported beam can be described by Eq. (2.19b), and the contribution of the kth mode to the displacement is

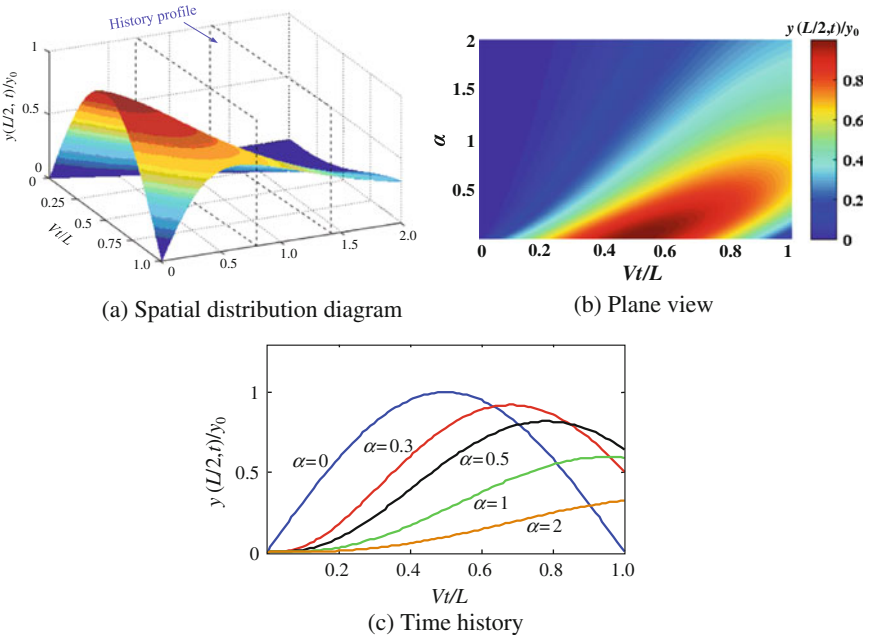

(a) Spatial distribution diagram

(b) Plane view

(c) Time history

Fig. 2.5 Distributions of mid-span displacement $y(L/2, t)/y_0$ versus time Vt/L and load speed α ($\mu = 1$)

$$y_k(x,t) = q_k(t)\sin\frac{k\pi x}{L} = y_0\frac{1}{k^2(k^2+\alpha^2)^2}\left\{(k^2-\alpha^2)\sin k\bar{\omega}t - 2k\alpha\cos k\bar{\omega}t + \mathrm{e}^{-\omega_k t}\left[(k^2+\alpha^2)k\bar{\omega}t + 2k\alpha\right]\right\}\sin\frac{k\pi x}{L} \tag{2.34}$$

When the bridge is critically damped, there is $\mu = \mu_{cr} = k^2$, which is not the critical damping for all the modes. When $n > k$, the nth mode is undercritically damped, and the corresponding generalized coordinate $q_n(t)$ can be solved by Eq. (2.17a). When $n < k$, the nth mode is overcritically damped, and the corresponding generalized coordinate $q_n(t)$ will be discussed in the next section.

Shown in Fig. 2.5a is the critically damped case, the spatial distribution of mid-span displacements of the bridge versus time parameter Vt/L, and load speed parameter α, in Fig. 2.5b is its plane view, and in Fig. 2.5c are the displacement time histories of the bridge related to various load speeds of $\alpha = 0, 0.3, 0.5, 1, 2$.

2.1.2.5 Overcritically Damped Case ($\mu > \mu_{cr} = k^2$)

According to the previous discussion, if the kth mode of the bridge is critically damped, the nth mode ($n < k$) will be overcritically damped, namely

$$\xi_n = \frac{\xi_k \omega_k}{\omega_n} = \frac{\omega_k}{\omega_n} > 1, \quad n < k \tag{2.35}$$

In the overcritically damped case, Eq. (2.12) is no longer valid, so the Duhamel integral solution to Eq. (2.11) becomes

$$q_n(t) = \frac{2}{\bar{m} L \omega_{\mathrm{D}}^n} \int_0^t P(\tau) \sin n\bar{\omega}\tau \cdot \mathrm{e}^{-\omega_{\mathrm{b}}(t-\tau)} \cdot \sinh \omega_{\mathrm{D}}^n (t-\tau) \mathrm{d}\tau \tag{2.36}$$

where $\omega_{\mathrm{D}}^n = \omega_n \sqrt{\xi_n^2 - 1}$ is the damped natural frequency of the nth mode, and $\sinh \omega_{\mathrm{D}}^n (t-\tau) = [\mathrm{e}^{\omega_{\mathrm{D}}^n (t-\tau)} - \mathrm{e}^{-\omega_{\mathrm{D}}^n (t-\tau)}]/2$.

The solution to the nth general coordinate is given by

$$\begin{aligned} q_n(t) = y_0 & \frac{1}{n^2[n^2(n^2-\alpha^2)^2 + 4\alpha^2\mu^2]} \left\{ n^2(n^2-\alpha^2) \sin n\bar{\omega}t - 2n\alpha\mu \cos n\bar{\omega}t \right. \\ & + \frac{n\alpha \mathrm{e}^{-\omega_{\mathrm{b}}t}}{2(\mu^2 - n^4)^{1/2}} \left\{ \left[2\mu^2 - n^2(n^2-\alpha^2) + 2\mu(\mu^2 - n^4)^{1/2} \right] \mathrm{e}^{\omega_{\mathrm{D}}^n t} \right. \\ & \left. \left. - \left[2\mu^2 - n^2(n^2-\alpha^2) - 2\mu(\mu^2 - n^4)^{1/2} \right] \mathrm{e}^{-\omega_{\mathrm{D}}^n t} \right\} \right\} \end{aligned} \tag{2.37}$$

and the displacement component of the simply-supported beam related to the nth ($n < k$) mode can be expressed as

$$\begin{aligned} y_n(x,t) = y_0 & \frac{1}{n^2[n^2(n^2-\alpha^2)^2 + 4\alpha^2\mu^2]} \left\{ n^2(n^2-\alpha^2) \sin n\bar{\omega}t - 2n\alpha\mu \cos n\bar{\omega}t \right. \\ & + \frac{n\alpha \mathrm{e}^{-\omega_{\mathrm{b}}t}}{2(\mu^2 - n^4)^{1/2}} \left\{ \left[2\mu^2 - n^2(n^2-\alpha^2) + 2\mu(\mu^2 - n^4)^{1/2} \right] \mathrm{e}^{\omega_{\mathrm{D}}^n t} \right. \\ & \left. \left. - \left[2\mu^2 - n^2(n^2-\alpha^2) - 2\mu(\mu^2 - n^4)^{1/2} \right] \mathrm{e}^{-\omega_{\mathrm{D}}^n t} \right\} \right\} \sin \frac{n\pi x}{L} \end{aligned} \tag{2.38}$$

Demonstrated in Fig. 2.6 is, in the overcritically damped ($\mu = 2$) case, the relationship between the relative displacement at the mid-span and the time parameter Vt/L and load speed parameter α.

2.1.3 Displacement of Bridge Subjected to a Moving Load Series

The analytical solutions above are valid for the bridge displacements induced by a single constant moving load. When performing dynamic analysis of the train-bridge system, the train load can be modeled as a moving load series composed of N loads

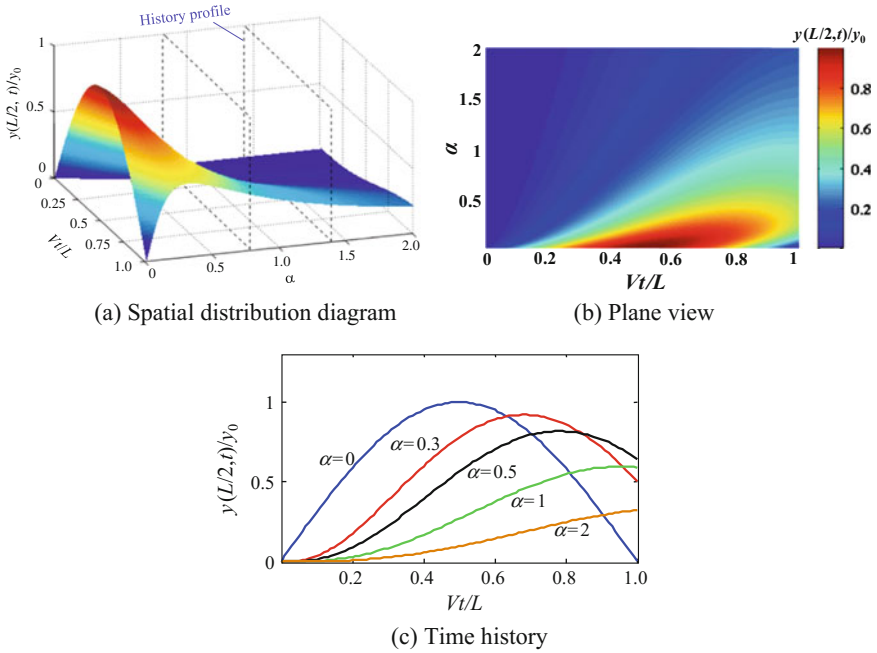

(a) Spatial distribution diagram (b) Plane view

(c) Time history

Fig. 2.6 Distributions of mid-span displacement $y(L/2, t)/y_0$ versus time Vt/L and load speed α ($\mu = 2$)

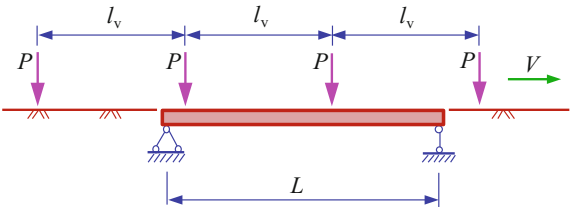

Fig. 2.7 Train load series moving on a simply-supported beam

with identical intervals equal to the vehicle length l_v, as shown in Fig. 2.7. By assuming small deformation for the beam, the displacement of the bridge under the load series can be directly written as the superposition of all responses induced by individual moving loads

$$y(x,t) = \sum_{i=0}^{N-1} y_i \left[x, \left(t - \frac{i \cdot l_v}{V} \right) \right] \tag{2.39}$$

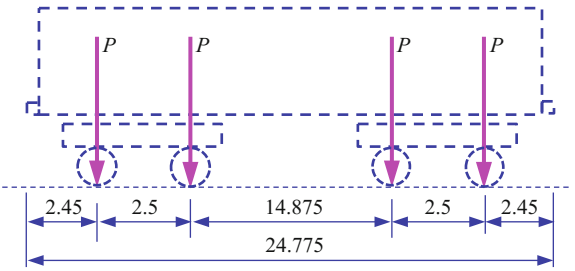

Fig. 2.8 Wheelbases of a German ICE3 car (Unit: m)

where $y_i(x, t)$ is the bridge displacement induced by the ith load of the moving load series.

Assuming the initial status of the bridge is still, the response of the bridge induced by each force of the moving load series can be analyzed in three phases. Before the force enters, the bridge does not vibrate, and $y_i(x, t)$ is zero. During the force moves on the beam, the bridge is in forced vibration, and $y_i(x, t)$ can be obtained by Eq. (2.19a, 2.19b). After the force leaves, the bridge is in free vibration, and $y_i(x, t)$ can be solved by Eq. (2.26).

Using the above method, the mid-span displacements of a simply-supported bridge under moving load series are calculated. The span of the bridge is $L = 32$ m, the fundamental frequency is $f_1 = 4.5$ Hz, and two damping ratios are considered as $\xi = 0, 0.05$, namely $\mu = 0, 0.05$. The moving load series consists of 32 concentrated forces, which are arranged according to the axle loads and wheelbases of the German ICE3 high-speed train composed of (3 motor-cars +1 trailer car) $\times$ 2, and each car has four wheel-sets, as shown in Fig. 2.8. The calculated displacement time histories of the bridge at mid-span are shown in Fig. 2.9.

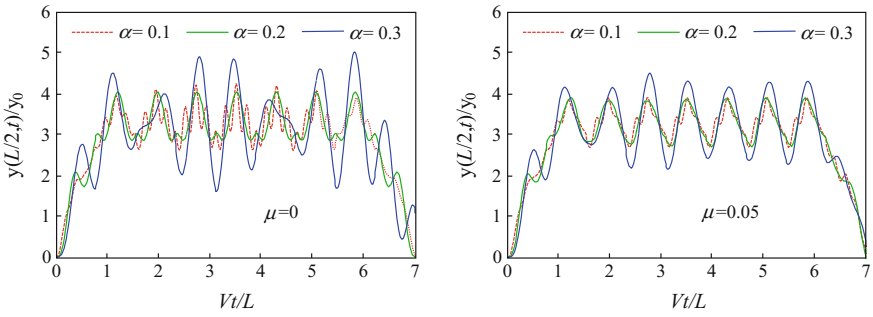

Fig. 2.9 Mid-span displacement time histories of the bridge

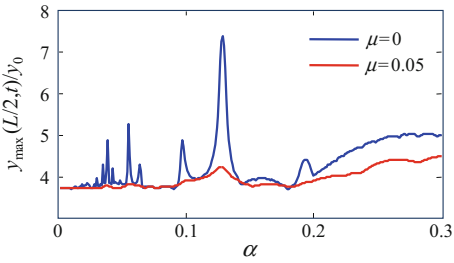

Fig. 2.10 Maximum defections at mid-span versus velocity and damping

Shown in Fig. 2.10 are the variations of maximum relative displacement $y_{\max}(L/2, t)/y_0$ of the bridge at mid-span versus load speed parameter α. It can be found that the periodic excitations by successive action of the concentrated force series induce several displacement peaks at certain speeds, indicating the resonant responses of the bridge, which are quite different from the regularity by a single moving load. The damping effect can reduce the maximum displacement and obviously depress the resonant response of the bridge. Detailed derivation of bridge resonance induced by moving load series can be found in Sect. 2.3.

2.1.4 *Analytical Solution for Vibration of Simply-Supported Beam Under a Moving Harmonic Load*

In this case, $P(t) = P \sin \theta t$, and thus, Eq. (2.12) can be expressed as

$$q_n(t) = \frac{2P}{\bar{m}L\omega_{\mathrm{D}}^n} \int_0^t \sin\theta\tau \sin n\bar{\omega}\tau \sin\omega_{\mathrm{D}}^n(t-\tau)\mathrm{e}^{-\omega_{\mathrm{b}}(t-\tau)}\mathrm{d}\tau \tag{2.40}$$

The following triangle transformation formula is utilized for the above integral

$$\begin{aligned}\sin\theta\tau \sin n\bar{\omega}\tau \sin\omega_{\mathrm{D}}^n(t-\tau) = \frac{1}{4}\{&\sin\left[\omega_{\mathrm{D}}^n t + \left(r_2 - \omega_{\mathrm{D}}^n\right)\tau\right] + \sin\left[\omega_{\mathrm{D}}^n t - \left(r_2 + \omega_{\mathrm{D}}^n\right)\tau\right] \\ &- \sin\left[\omega_{\mathrm{D}}^n t + \left(r_1 - \omega_{\mathrm{D}}^n\right)\tau\right] - \sin\left[\omega_{\mathrm{D}}^n t - \left(r_1 + \omega_{\mathrm{D}}^n\right)\tau\right]\}\end{aligned} \tag{2.41}$$

where $r_1 = \theta + n\bar{\omega}$, and $r_2 = \theta - n\bar{\omega}$.

Substituting Eq. (2.41) into Eq. (2.40), and using Eq. (2.15a, 2.15b), the precise integral solution of Eq. (2.40) can be deduced as

$$
\begin{aligned}
q_n(t) &= \frac{P}{2\bar{m}L\omega_{\mathrm{D}}^n}\left\{\int_0^t \sin\left[\omega_{\mathrm{D}}^n t + (r_2-\omega_{\mathrm{D}}^n)\tau\right]\mathrm{e}^{-\omega_{\mathrm{b}}(t-\tau)}\mathrm{d}\tau + \int_0^t \sin\left[\omega_{\mathrm{D}}^n t - (r_2+\omega_{\mathrm{D}}^n)\tau\right]\mathrm{e}^{-\omega_{\mathrm{b}}(t-\tau)}\mathrm{d}\tau\right. \\
&\quad \left. - \int_0^t \sin\left[\omega_{\mathrm{D}}^n t + (r_1-\omega_{\mathrm{D}}^n)\tau\right]\mathrm{e}^{-\omega_{\mathrm{b}}(t-\tau)}\mathrm{d}\tau - \int_0^t \sin\left[\omega_{\mathrm{D}}^n t - (r_1+\omega_{\mathrm{D}}^n)\tau\right]\mathrm{e}^{-\omega_{\mathrm{b}}(t-\tau)}\mathrm{d}\tau\right\} \\
&= \frac{P}{2\bar{m}L\omega_{\mathrm{D}}^n}\left\{\frac{1}{(r_2-\omega_{\mathrm{D}}^n)^2+\omega_{\mathrm{b}}^2}\left\{\left[\omega_{\mathrm{b}}\sin r_2 t - (r_2-\omega_{\mathrm{D}}^n)\cos r_2 t\right] - \left[\omega_{\mathrm{b}}\sin\omega_{\mathrm{D}}^n t - (r_2-\omega_{\mathrm{D}}^n)\cos\omega_{\mathrm{D}}^n t\right]\mathrm{e}^{-\omega_{\mathrm{b}}t}\right\}\right. \\
&\quad + \frac{1}{(r_2+\omega_{\mathrm{D}}^n)^2+\omega_{\mathrm{b}}^2}\left\{\left[-\omega_{\mathrm{b}}\sin r_2 t + (r_2+\omega_{\mathrm{D}}^n)\cos r_2 t\right] - \left[\omega_{\mathrm{b}}\sin\omega_{\mathrm{D}}^n t + (r_2+\omega_{\mathrm{D}}^n)\cos\omega_{\mathrm{D}}^n t\right]\mathrm{e}^{-\omega_{\mathrm{b}}t}\right\} \\
&\quad - \frac{1}{(r_1-\omega_{\mathrm{D}}^n)^2+\omega_{\mathrm{b}}^2}\left\{\left[\omega_{\mathrm{b}}\sin r_1 t - (r_1-\omega_{\mathrm{D}}^n)\cos r_1 t\right] - \left[\omega_{\mathrm{b}}\sin\omega_{\mathrm{D}}^n t - (r_1-\omega_{\mathrm{D}}^n)\cos\omega_{\mathrm{D}}^n t\right]\mathrm{e}^{-\omega_{\mathrm{b}}t}\right\} \\
&\quad \left. - \frac{1}{(r_1+\omega_{\mathrm{D}}^n)^2+\omega_{\mathrm{b}}^2}\left\{\left[-\omega_{\mathrm{b}}\sin r_1 t + (r_1+\omega_{\mathrm{D}}^n)\cos r_1 t\right] - \left[\omega_{\mathrm{b}}\sin\omega_{\mathrm{D}}^n t + (r_1+\omega_{\mathrm{D}}^n)\cos\omega_{\mathrm{D}}^n t\right]\mathrm{e}^{-\omega_{\mathrm{b}}t}\right\}\right\}
\end{aligned}
\tag{2.42}
$$

In the undercritically damped case, $\omega_{\mathrm{D}}^{n2} = \omega_n^2 - \omega_{\mathrm{b}}^2$, Eq. (2.42) can be rearranged as

$$
\begin{aligned}
q_n(t) = \frac{P}{\bar{m}L}&\left\{\frac{1}{(\omega_n^2-r_2^2)^2+4\omega_{\mathrm{b}}^2 r_2^2}\left[(\omega_n^2-r_2^2)\left(\cos r_2 t - \mathrm{e}^{-\omega_{\mathrm{b}}t}\cos\omega_{\mathrm{D}}^n t\right)\right.\right. \\
&\left. + 2\omega_{\mathrm{b}} r_2 \sin r_2 t - \frac{\omega_{\mathrm{b}}}{\omega_{\mathrm{D}}^n}(\omega_n^2+r_2^2)\mathrm{e}^{-\omega_{\mathrm{b}}t}\sin\omega_{\mathrm{D}}^n t\right] \\
&- \frac{1}{(\omega_n^2-r_1^2)^2+4\omega_{\mathrm{b}}^2 r_1^2}\left[(\omega_n^2-r_1^2)\left(\cos r_1 t - \mathrm{e}^{-\omega_{\mathrm{b}}t}\cos\omega_{\mathrm{D}}^n t\right)\right. \\
&\left.\left. + 2\omega_{\mathrm{b}} r_1 \sin r_1 t - \frac{\omega_{\mathrm{b}}}{\omega_{\mathrm{D}}^n}(\omega_n^2+r_1^2)\mathrm{e}^{-\omega_{\mathrm{b}}t}\sin\omega_{\mathrm{D}}^n t\right]\right\}
\end{aligned}
\tag{2.43}
$$

Based on the generalized coordinates obtained from Eq. (2.43), the particular solution for the displacement of the simply-supported beam under a moving harmonic load can be written as

$$
\begin{aligned}
y(x,t) = \frac{y_0}{2}\sum_{n=1}^{\infty}&\left\{\frac{\omega_1^2}{(\omega_n^2-r_2^2)^2+4\omega_{\mathrm{b}}^2 r_2^2}\left[(\omega_n^2-r_2^2)\left(\cos r_2 t - \mathrm{e}^{-\omega_{\mathrm{b}}t}\cos\omega_{\mathrm{D}}^n t\right)\right.\right. \\
&\left. + 2\omega_{\mathrm{b}} r_2 \sin r_2 t - \frac{\omega_{\mathrm{b}}}{\omega_{\mathrm{D}}^n}(\omega_n^2+r_2^2)\mathrm{e}^{-\omega_{\mathrm{b}}t}\sin\omega_{\mathrm{D}}^n t\right] \\
&- \frac{\omega_1^2}{(\omega_n^2-r_1^2)^2+4\omega_{\mathrm{b}}^2 r_1^2}\left[(\omega_n^2-r_1^2)\left(\cos r_1 t - \mathrm{e}^{-\omega_{\mathrm{b}}t}\cos\omega_{\mathrm{D}}^n t\right)\right. \\
&\left.\left. + 2\omega_{\mathrm{b}} r_1 \sin r_1 t - \frac{\omega_{\mathrm{b}}}{\omega_{\mathrm{D}}^n}(\omega_n^2+r_1^2)\mathrm{e}^{-\omega_{\mathrm{b}}t}\sin\omega_{\mathrm{D}}^n t\right]\right\}\sin\frac{n\pi x}{L}
\end{aligned}
\tag{2.44}
$$

in which $q_n(t)$ is the generalized coordinate of the nth mode.

According to engineering practice, some additional conditions are herein introduced to simplify Eq. (2.44). For example, for solution of bridge displacement, sufficiently precise can be obtained by considering the first-order mode, so only

$n = 1$ is taken. For a real bridge, the dimensionless parameters α and μ are usually very small, i.e., $\alpha \ll 1$ and $\mu \ll 1$. Accordingly, Eq. (2.44) can be rewritten as

$$y(x,t) = y_0 \frac{\omega_1^2}{\theta^2} \frac{1}{\left(\frac{\omega_1^2}{\theta^2} - 1\right)^2 + 4\left(\frac{\bar{\omega}^2}{\theta^2} + \frac{\omega_b^2}{\theta^2}\right)} \left\{ \left[\left(\frac{\omega_1^2}{\theta^2} - 1\right)^2 + 4\frac{\omega_b^2}{\theta^2} \right]^{1/2} \sin(\theta t + \varphi) \sin \bar{\omega} t \right.$$
$$\left. + 2\frac{\bar{\omega}}{\theta}(\cos\theta t \cos\bar{\omega} t - e^{-\omega_b t} \cos\omega_1 t) \right\} \sin\frac{\pi x}{L} \tag{2.45}$$

where $\varphi = \tan^{-1}\left(-\frac{2\omega_b/\theta}{\omega_1^2/\theta^2 - 1}\right)$.

To better describe the frequency effect of the harmonic load, a dimensionless parameter, frequency ratio, is introduced, expressed as

$$\gamma = \frac{\theta}{\omega_1} \tag{2.46}$$

where θ is the frequency of the harmonic load, and μ_1 is the fundamental frequency of the bridge.

Under $\mu = 0.05$ and various frequency ratios, the distributions of mid-span displacement $y(L/2, t)/y_0$ of the bridge versus time parameter Vt/L and load speed parameter α are shown in Fig. 2.11.

According to Eq. (2.46), when the loading frequency θ is close or equal to the first-order frequency ω_1 of the bridge, the maximum bridge dynamic response can be observed. In this case, Eq. (2.45) can be rewritten as

$$y(x,t) = y_0 \frac{\omega_1}{2} \frac{\cos\omega_1 t}{\bar{\omega}^2 + \omega_b^2} [\omega(\cos\bar{\omega} t - e^{-\omega_b t}) - \omega_b \sin\bar{\omega} t] \sin\frac{\pi x}{L} \tag{2.47}$$

Dynamic amplification factor

Herein, the dynamic amplification factor (DAF) is defined as the ratio of the maximum mid-span deflection of the bridge caused by the moving harmonic load $P(t) = P \sin\theta t$ to the deflection induced by the static load P, denoted as

$$D_{1/2} = \frac{\max[y(L/2, t)]}{y_0} \tag{2.48}$$

To investigate the variations of the bridge DAF versus loading frequency ratio γ and load speed parameter α, the maximum mid-span displacements of the bridge are calculated, considering different loading frequencies and load speeds in the undercritically damped case ($\mu = 0.05$), and the results are shown in Fig. 2.12.

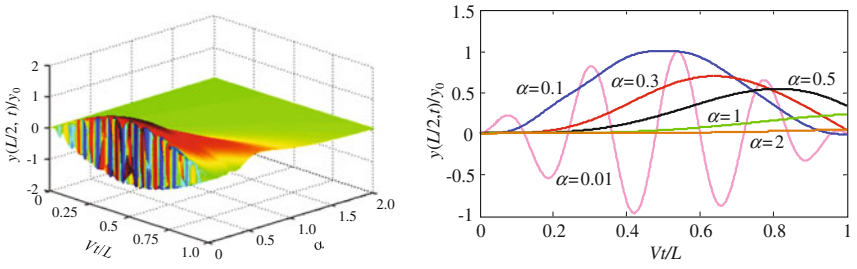

(a) $\gamma = 0.1$

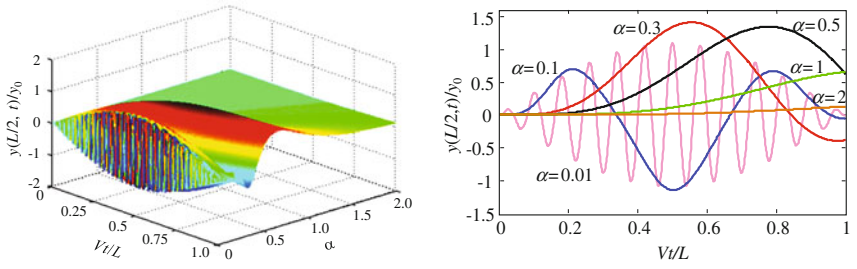

(b) $\gamma = 0.3$

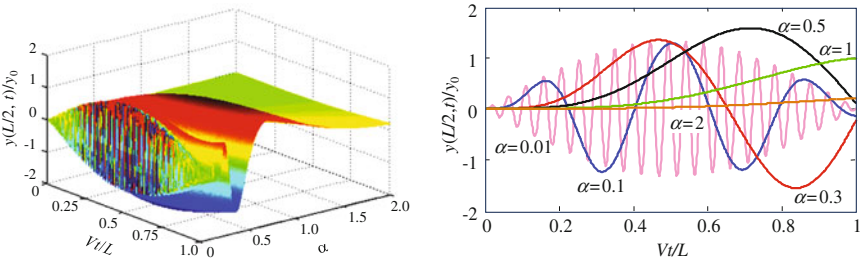

(c) $\gamma = 0.5$

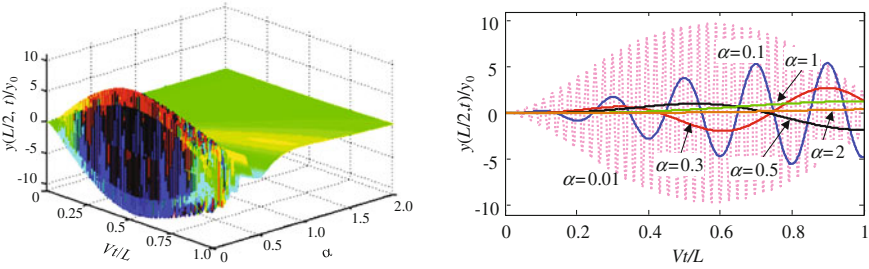

(d) $\gamma = 1.0$

Fig. 2.11 Distributions of mid-span displacement $y(L/2, t)/y_0$ of the bridge versus Vt/L and α under a harmonic load with various frequencies ($\mu = 0.05$)

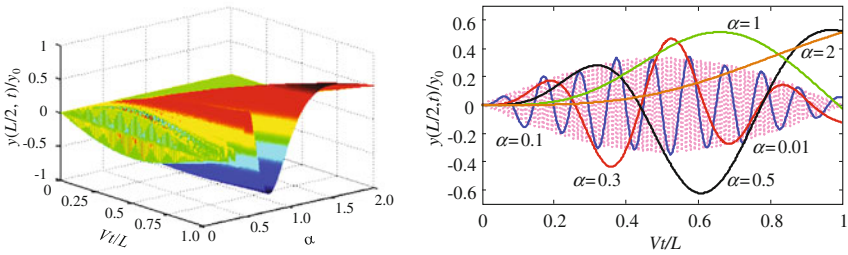

(e) γ = 2.0

Fig. 2.11 (continued)

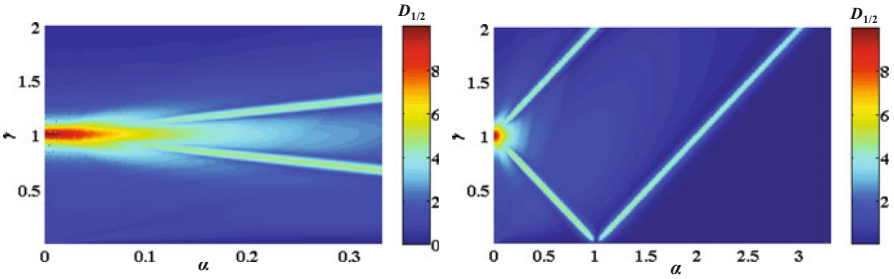

(a) $\alpha = 0 \sim 0.3$ (b) $\alpha = 0 \sim 3$

Fig. 2.12 Variations of bridge DAF versus loading frequency ratio γ and speed parameter α ($\mu = 0.05$)

It can be found that when the load speed is small, the loading frequency has little influence, and thus, the displacement response is similar to that under static load and reaches the maximum at $\gamma = 1$. With the increase of load speed, the influence of loading frequency on bridge displacement enlarges, the bridge DAF at $\gamma = 1$ gradually decreases, and the loading frequency corresponding to the maximum DAF changes, no longer at $\gamma = 1$.

An interesting phenomenon associated with the bridge displacement response can be observed in Fig. 2.12b. Considering the two axis planes as a mirror, the line connecting the maximum displacement points is equivalent to a ray with 45° incident, producing a peak displacement at the intersection position ($\alpha = 0$, $\gamma = 1$) with the mirror. This phenomenon is called the ray reflection effect of the maximum displacement response. In the figure, $D_{1/2}$ is nearly zero when γ is around null (i.e., $\theta \approx 0$), since $P(t) = P \sin \theta t \approx 0$. Hence, the displacement induced by a moving constant load cannot be directly obtained from Eq. (2.44) for the moving harmonic load by setting $\gamma = 0$.

2.2 Vibration of Simply-Supported Beam Under Moving Loads with Variable Speed

In the previous sections, the analysis method and the dynamic response characteristics of a simply-supported beam under moving concentrated load and harmonic load were introduced, and in Xia and Zhang (2005) and Xia et al. (2012), the cases considering moving uniformly distributed mass and the moving vehicle with sprung-mass were discussed. All the above-mentioned loads are moving at constant speed, while in fact, moving vehicles are usually subjected to acceleration and deceleration. In this section, the investigation is extended to a more general case, i.e., the vibration of a simply-supported beam subjected to a moving wheel-spring-mass (WSM) load with variable speed.

2.2.1 *Calculation Model*

The calculation model of the simply-supported beam under a moving WSM load with variable speed is shown in Fig. 2.13. The moving WSM load is composed of a wheel (unsprung-mass) M_1, a sprung-mass M_2, a spring k_1, and a dashpot c_1.

In the analysis, the initial speed of the load is V_0, the acceleration is $a(t)$, the speed at time t is $V(t)$, the moved distance is $s(t)$, the dynamic deflection of the beam is $y(x, t)$, and the movement of the sprung-mass M_2 is $Z(t)$. By assuming the wheel M_1 moves along the beam without detachment, the deflection of the wheel M_1 is consistent with that of the beam at the position of the wheel.

The sprung-mass M_2 is subjected to the inertial force $P_{I2} = M_2\ddot{Z}(t)$, the elastic force $P_S = k_1[Z(t) - y(x,t)]|_{x=s(t)}$ due to the relative displacement between M_2 and M_1, and the damping force $P_D' = c_1[\dot{Z}(t) - \dfrac{\mathrm{d}y(x,t)}{\mathrm{d}t}]|_{x=s(t)}$ due to the relative velocity between M_2 and M_1. By considering the equilibrium of forces on M_2 shown in Fig. 2.13, the motion equation for the sprung-mass M_2 can be derived as

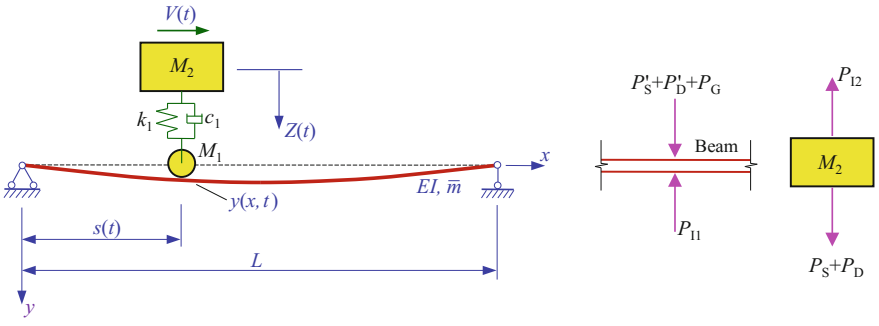

Fig. 2.13 Model of simply-supported bridge with a speed-varying WSM load

$$M_2\ddot{Z}(t)+k_1\left[Z(t)-y(x,t)|_{x=s(t)}\right]+c_1\left[\dot{Z}(t)-\frac{\mathrm{d}y(x,t)}{\mathrm{d}t}\bigg|_{x=s(t)}\right]=0 \tag{2.49}$$

where $\dfrac{\mathrm{d}y}{\mathrm{d}t}=\dfrac{\partial y(x,t)}{\partial t}+\dfrac{\partial y(x,t)}{\partial x}V(t)$. Since the load speed is not constant, both terms should be considered. The motion equation of the mass M_2 becomes

$$M_2\ddot{Z}(t)+k_1[Z(t)-y(x,t)|_{x=s(t)}]+c_1\left\{\dot{Z}(t)-\left[\frac{\partial y(x,t)}{\partial t}+\frac{\partial y(x,t)}{\partial x}V(t)\right]\bigg|_{x=s(t)}\right\}=0 \tag{2.50}$$

When the WSM load moves on the beam at the speed of $V(t)$, the beam is subjected to the inertial force $P_{\mathrm{I1}}=M_1\dfrac{\mathrm{d}^2y(t)}{\mathrm{d}t^2}|_{x=s(t)}$ from the mass M_1, the gravity $P_{\mathrm{G}}=(M_1+M_2)g$ of the masses, the elastic force $P_{\mathrm{S}}^{'}=P_{\mathrm{S}}$, and the damping force $P_{D}^{'}=P_{\mathrm{D}}$. Thus, the force applied on the beam can be expressed as

$$\begin{aligned}P(x,t)&=\delta[x-s(t)][P_{\mathrm{G}}-P_{\mathrm{I}}+P_{\mathrm{S}}+P_{\mathrm{D}}]\\&=\delta[x-s(t)]\left\{(M_1+M_2)g-M_1\frac{\mathrm{d}^2y(x,t)}{\mathrm{d}t^2}+k_1[Z(t)-y(x,t)]+c_1\left[\dot{Z}(t)-\frac{\mathrm{d}y(x,t)}{\mathrm{d}t}\right]\right\}\end{aligned} \tag{2.51}$$

Note that $\dfrac{\mathrm{d}^2y}{\mathrm{d}t^2}=\dfrac{\partial^2y}{\partial t^2}+2\dfrac{\partial^2y}{\partial x\partial t}V(t)+\dfrac{\partial y}{\partial x}a(t)+\dfrac{\partial^2y}{\partial x^2}V^2(t),\dfrac{\mathrm{d}y}{\mathrm{d}t}=\dfrac{\partial y(x,t)}{\partial t}+\dfrac{\partial y(x,t)}{\partial x}V(t)$, and $a(t)=\frac{\mathrm{d}V(t)}{\mathrm{d}t}$ is the moving acceleration of the load, and Eq. (2.51) can be rewritten as

$$\begin{aligned}P(x,t)=\delta[x-s(t)]\Bigg\{&(M_1+M_2)g-M_1\left[\frac{\partial^2y(x,t)}{\partial t^2}+2\frac{\partial^2y(x,t)}{\partial x\partial t}V(t)+\frac{\partial y(x,t)}{\partial x}a(t)\right.\\&\left.+\frac{\partial^2y(x,t)}{\partial x^2}V^2(t)\right]+k_1[Z(t)-y(x,t)]+c_1\left\{\dot{Z}(t)-\left[\frac{\partial y(x,t)}{\partial t}+\frac{\partial y(x,t)}{\partial x}V(t)\right]\right\}\Bigg\}\end{aligned} \tag{2.52}$$

The motion equation of the simply-supported beam under loads with variable speed can be expressed as

$$EI\frac{\partial^4y(x,t)}{\partial x^4}+\bar{m}\frac{\partial^2y(x,t)}{\partial t^2}+c\frac{\partial y(x,t)}{\partial t}=P(x,t) \tag{2.53}$$

When Eq. (2.53) is solved with the modal decomposition method, by substituting $y(x,t) = \sum_{i=1}^{\infty} q_i(t) \cdot \phi_i(x)$ into the equation, multiplying each term by the mode shape function $\phi_n(x) = \sin\frac{n\pi x}{L}$, integrating along the beam, and considering the orthogonality of modes, Eq. (2.53) becomes

$$\ddot{q}_n(t) + 2\xi_n\omega_n\dot{q}_n(t) + \omega_n^2 q_n(t) = \frac{2}{\bar{m}L}P_n(t) \quad (n = 1, 2, \ldots\ldots) \tag{2.54}$$

in which $P_n(t)$ is the generalized force of the nth mode, expressed as

$$P_n(t) = P_{n1}(t) + P_{n2}(t) \tag{2.55}$$

where

$$\begin{aligned} P_{n1}(t) &= \int_0^L \delta[x - s(t)]\left\{(M_1 + M_2)g - M_1\left[\sum_{i=1}^{\infty}\ddot{q}_i(t)\phi_i(x) + 2\sum_{i=1}^{\infty}\dot{q}_i(t)\phi_i'(x)V(t)\right.\right. \\ &\quad \left.\left. + \sum_{i=1}^{\infty} q_i(t)\phi_i'(x)a(t) + \sum_{i=1}^{\infty} q_i(t)\phi_i''(x)V^2(t)\right]\right\}\phi_n(t)\mathrm{d}x \\ &= (M_1 + M_2)g\,\sin\frac{n\pi s(t)}{L} - M_1\sum_{i=1}^{\infty}\ddot{q}_i(t)\left[\frac{i\pi}{L}a(t)\cos\frac{i\pi s(t)}{L} - \left(\frac{i\pi}{L}\right)^2 V^2(t)\sin\frac{i\pi s(t)}{L}\right] \\ &\quad \times \sin\frac{n\pi s(t)}{L} - 2M_1\sum_{i=1}^{\infty}\dot{q}_i(t)\frac{i\pi}{L}V(t)\cos\frac{i\pi s(t)}{L}\sin\frac{n\pi s(t)}{L} \\ &\quad - M_1\sum_{i=1}^{\infty}\ddot{q}_i(t)\sin\frac{i\pi s(t)}{L}\sin\frac{n\pi s(t)}{L} \end{aligned} \tag{2.56a}$$

$$\begin{aligned} P_{n2}(t) &= \int_0^L \delta[x - s(t)]\left\{k_1 Z(t) + c_1\dot{Z}(t)\right. \\ &\quad \left. - \sum_{i=1}^{\infty}\left\{k_1 q_i(t)\phi_i(x) + c_1\left[\dot{q}_i(t)\phi_i(x) + q_i(t)\phi_i'(x)V(t)\right]\right\}\right\}\phi_n(x)\mathrm{d}x \\ &= \left[k_1 z(t) + c_1\dot{Z}(t)\right]\sin\frac{n\pi s(t)}{L} - \sum_{i=1}^{\infty}\dot{q}_i(t)c_1\sin\frac{i\pi s(t)}{L}\sin\frac{n\pi s(t)}{L} \\ &\quad - \sum_{i=1}^{\infty} q_i(t)\left[k_1\sin\frac{i\pi s(t)}{L} + c_1 V(t)\cos\frac{i\pi s(t)}{L}\right]\sin\frac{n\pi s(t)}{L} \end{aligned} \tag{2.56b}$$

By moving the unknown displacement, velocity, and acceleration terms from the right-hand side of Eq. (2.52) to the left, the following equation can be obtained

$$\begin{aligned}
&\ddot{q}_n(t)+\frac{2M_1}{\bar{m}L}\sum_{i=1}^{\infty}\ddot{q}_i(t)\sin\frac{i\pi s(t)}{L}\sin\frac{n\pi s(t)}{L}+2\xi_n\omega_n\dot{q}_n(t)\\
&\quad+\frac{2c_1}{\bar{m}L}\sum_{i=1}^{\infty}\dot{q}_i(t)\sin\frac{i\pi s(t)}{L}\sin\frac{n\pi s(t)}{L}+\frac{4M_1}{\bar{m}L}\sum_{i=1}^{\infty}\dot{q}_i(t)\frac{i\pi}{L}V(t)\cos\frac{i\pi s(t)}{L}\sin\frac{n\pi s(t)}{L}\\
&\quad+\omega_n^2q_n(t)+\frac{2M_1}{\bar{m}L}\sum_{i=1}^{\infty}q_i(t)\left[\frac{i\pi}{L}a(t)\cos\frac{i\pi s(t)}{L}\sin\frac{n\pi s(t)}{L}-\left(\frac{i\pi}{L}\right)^2V^2(t)\sin\frac{i\pi s(t)}{L}\sin\frac{n\pi s(t)}{L}\right]\\
&\quad+\frac{2k_1}{\bar{m}L}\sum_{i=1}^{\infty}q_i(t)\sin\frac{i\pi s(t)}{L}\sin\frac{n\pi s(t)}{L}+\frac{2c_1}{\bar{m}L}\sum_{i=1}^{\infty}q_i(t)\frac{i\pi}{L}V(t)\cos\frac{i\pi s(t)}{L}\sin\frac{n\pi s(t)}{L}\\
&\quad-\frac{2}{\bar{m}L}\left[k_1Z(t)+c_1\dot{Z}(t)\right]\sin\frac{n\pi s(t)}{L}\\
&=\frac{2}{\bar{m}L}(M_1+M_2)g\sin\frac{n\pi s(t)}{L}
\end{aligned}\tag{2.57}$$

When the bridge displacement at the load position is expressed with the modal decomposition method, the motion equation of the sprung-mass M_2 becomes

$$\begin{aligned}
&M_2\ddot{Z}(t)+c_1\dot{Z}(t)+k_1Z(t)-c_1\sum_{i=1}^{\infty}\dot{q}_i(t)\sin\frac{i\pi s(t)}{L}\\
&\quad-c_1\sum_{i=1}^{\infty}q_i(t)\frac{i\pi}{L}V(t)\cos\frac{i\pi s(t)}{L}-k_1\sum_{i=1}^{\infty}q_i(t)\sin\frac{i\pi s(t)}{L}=0
\end{aligned}\tag{2.58}$$

The motion equation of the system can be obtained by combining Eqs. (2.57) and (2.58). For a simply-supported beam, if N terms of displacement series are used, and the sprung-mass M_2 has one DOF $Z(t)$, the motion equations of the system can be expressed in terms of matrices with $(N + 1)$ orders as

$$\mathbf{M}\{\ddot{X}\}+\mathbf{C}\{\dot{X}\}+\mathbf{K}\{X\}=\{F\}\tag{2.59}$$

where $\{X\}$ is the generalized displacement vector; **M**, **C,** and **K** are the generalized mass, damping, and stiffness matrices, respectively; and $\{F\}$ is the generalized load vector. They are expressed as follows

$$\{X\}=[q_1(t),q_2(t),\cdots,q_N(t),Z(t)]^{\mathrm{T}}\tag{2.60}$$

$$\mathbf{M}=\begin{bmatrix}
1+\rho_{\mathrm{M}}\Phi_{11} & \rho_{\mathrm{M}}\Phi_{12} & \cdots & \rho_{\mathrm{M}}\Phi_{1N} & 0\\
\rho_{\mathrm{M}}\Phi_{21} & 1+\rho_{\mathrm{M}}\Phi_{22} & \cdots & \rho_{\mathrm{M}}\Phi_{2N} & 0\\
\cdots & \cdots & \ddots & \cdots & 0\\
\rho_{\mathrm{M}}\Phi_{N1} & \rho_{\mathrm{M}}\Phi_{N2} & \cdots & 1+\rho_{\mathrm{M}}\Phi_{NN} & 0\\
0 & 0 & 0 & 0 & M_2
\end{bmatrix}\tag{2.61}$$

$$\mathbf{C}=\begin{bmatrix} 2\xi_1\omega_1+\varphi_{11}+\rho_C\Phi_{11} & \varphi_{12}+\rho_C\Phi_{12} & \cdots & \varphi_{1N}+\rho_C\Phi_{1N} & -\rho_C\phi_1 \\ \varphi_{21}+\rho_C\Phi_{21} & 2\xi_2\omega_2+\varphi_{22}+\rho_C\Phi_{22} & \cdots & \varphi_{2N}+\rho_C\Phi_{2N} & -\rho_C\phi_2 \\ \cdots & \cdots & \ddots & \cdots & \cdots \\ \varphi_{N1}+\rho_C\Phi_{N1} & \varphi_{N2}+\rho_C\Phi_{N2} & \cdots & 2\xi_N\omega_N+\varphi_{NN}+\rho_C\Phi_{NN} & -\rho_C\phi_N \\ -c_1\phi_1 & -c_1\phi_2 & \cdots & -c_1\phi_N & c_1 \end{bmatrix} \tag{2.62}$$

$$\mathbf{K}=\begin{bmatrix} \omega_1^2+\psi_{11}+\rho_K\Phi_{11} & \psi_{12}+\rho_K\Phi_{12} & \cdots & \psi_{1N}+\rho_K\Phi_{1N} & -\rho_K\phi_1 \\ \psi_{21}+\rho_K\Phi_{21} & \omega_2^2+\psi_{22}+\rho_K\Phi_{22} & \cdots & \psi_{2N}+\rho_K\Phi_{2N} & -\rho_K\phi_2 \\ \cdots & \cdots & \ddots & \cdots & \cdots \\ \psi_{N1}+\rho_K\Phi_{N1} & \psi_{N2}+\rho_K\Phi_{N2} & \cdots & \omega_N^2+\psi_{NN}+\rho_K\Phi_{NN} & -\rho_K\phi_N \\ \Gamma_1-k_1\phi_1 & \Gamma_2-k_1\phi_2 & \cdots & \Gamma_N-k_1\phi_N & k_1 \end{bmatrix} \tag{2.63}$$

$$\{F\}=[\rho_F\phi_1,\ \rho_F\phi_2,\ \cdots,\ \rho_F\phi_N,\ 0]^T \tag{2.64}$$

where:

$\rho_M=\frac{2M_1}{\bar{m}L}, \rho_C=\frac{2c_1}{\bar{m}L}, \rho_K=\frac{2k_1}{\bar{m}L}, \rho_F=\frac{2(M_1+M_2)}{\bar{m}L}g, \phi_n=\sin\frac{n\pi s(t)}{L}, \Phi_{nm}=\phi_n\phi_m,$
$\beta_n=\cos\frac{n\pi s(t)}{L}, \varphi_{nm}=\frac{2m\pi}{L}\rho_M\phi_n\beta_m V(t), \Gamma_n=-c_nV(t)\frac{n\pi}{L}\beta_n,$ and
$\psi_{nm}=\rho_M\left[\frac{m\pi}{L}\phi_n\beta_m a(t)-\frac{m^2\pi^2}{L^2}V^2(t)\Phi_{nm}\right]+\frac{m\pi}{L}\rho_C V(t)\phi_n\beta_m.$

The multiplier φ_{nm} in the damping matrix and ψ_{nm} and Γ_n in the stiffness matrix represent the influence of variable speed of the moving load.

The results show that for the simply-supported beam subjected to a moving WSM load, the generalized mass matrix **M** is non-diagonal, but the coupling terms with M_2 are zeros. Both **K** and **C** are non-diagonal full matrices, through which the equations for the beam and the moving load are coupled. Although the equations for the whole system cannot be completely decoupled by modal decomposition, the order of the equations can be reduced by adopting an appropriate order number N.

Since the WSM load is moving on the beam, the coefficients Φ_{nm}, φ_{nm}, $\psi_{nm,}$ and Γ_n in the generalized mass matrix **M**, stiffness matrix **K,** and damping matrix **C** are time-varying. Therefore, Eq. (2.59) is a second-order linear differential equations with time-varying coefficients, which is usually solved by the step-by-step numerical integration method.

2.2.2 Case Study

Based on the above theory and analysis method, a computation program is developed to analyze the dynamic response of a three-span simply-supported bridge subjected to a moving WSM load with constant acceleration.

The bridge consists of 3×32 m PC box-beams. The beam is made of C50 concrete with elastic modulus of 34.5 MPa and mass density of 2500 kg/m^3.

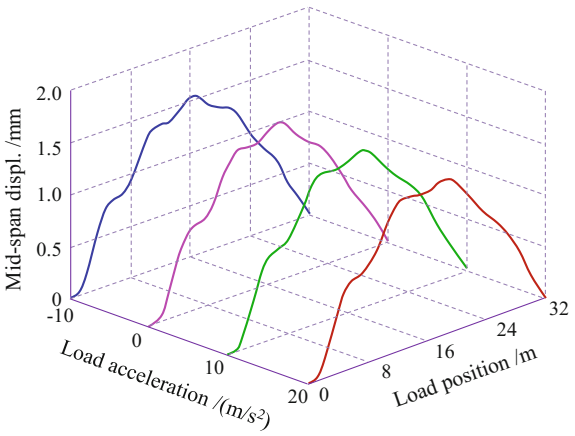

Fig. 2.14 Displacement time histories of the bridge under the speed-varying WSM load

The cross section of the beam has an area of 8.97 m^2 and an inertia moment of 11.1 m^4. In the WSM model, the wheel mass M_1 is 10.68 t, the sprung-mass M_2 is 73.32 t, the spring coefficient k_1 is 7.48 MN/m, and the damping coefficient c_1 is 240 kNs/m.

In the calculation, the first five vibration modes are considered for the bridge, the damping ratio is 0.05, the Newmark parameters are $\lambda = 0.5$ and $\beta = 0.25$, and the integration time step is 0.0005 s.

Shown in Fig. 2.14 are the dynamic displacement histories of the bridge at the central mid-span, when the WSM load enters the bridge at initial speed of 40 m/s and then moves on the bridge at a constant speed, variable speeds with accelerations of 10 m/s^2, 20 m/s^2, and -10 m/s^2, respectively. It can be observed that when the load moves on the bridge with different accelerations, the displacement time history curves are quite similar, but the maximum displacements are slightly different.

To further investigate the influence of load moving acceleration, some representative points on the maximum displacement curve of the bridge versus load moving speed are discussed in detail. The load speeds are divided into four categories according to the variation feature of the curve, as shown in Fig. 2.15, which are represented by speed points 1–6. Listed in Table 2.1 are the initial speeds, the accelerations of the load, and the maximum mid-span displacements of the bridge adopted in the calculation.

Based on Fig. 2.15 and the calculated results in Table 2.1, the influences of speed variations at these points on bridge maximum displacements are analyzed from the view of load-bridge resonance.

(1) Category I. Points 1 and 4 belong to this category, which are the load speeds yielding peak displacement responses. Corresponding to these points, when the load arrives at the mid-span, the speeds do not equal those yielding the maximum displacements; thus, in both the acceleration and deceleration cases, the maximum displacements become smaller.

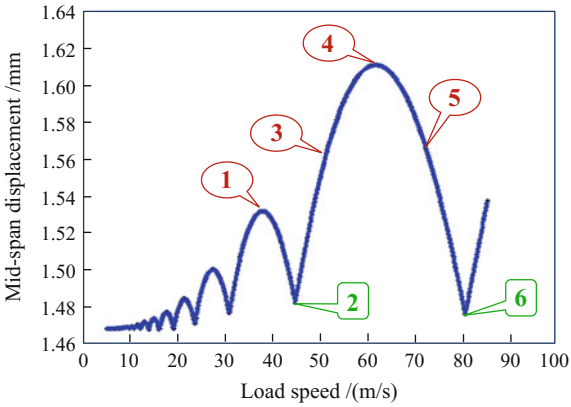

Fig. 2.15 Calculated representative load speeds

Table 2.1 Maximum displacements of bridge under speed-varying WSM load

Item		Maximum displacement (mm)					
Point number		1	2	3	4	5	6
Category		I	II	III	I	IV	II
Initial speed V_0 (m/s)		37.8	44.6	50.0	61.5	72.0	80.0
Acceleration a (m/s^2)	0	1.532	1.482	1.552	1.611	1.566	1.476
	5	1.530	1.492	1.558	1.610	1.560	1.479
	10	1.526	1.502	1.564	1.609	1.554	1.484
	15	1.519	1.502	1.570	1.608	1.548	1.488
Deceleration a (m/s^2)	0	1.532	1.482	1.552	**1.611**	1.566	1.476
	−5	1.531	1.496	1.545	**1.612**	1.572	1.484
	−10	1.528	1.508	1.534	**1.612**	1.577	1.493
	−15	1.522	1.518	1.529	**1.611**	1.582	1.501

(2) Category II. Points 2 and 6 belong to this category, which are the load speeds yielding valley displacement responses. Corresponding to these points, when the load arrives at the mid-span, the speeds do not equal those yielding the minimum displacements; thus, in both the acceleration and deceleration cases, the maximum displacements become larger.

(3) Category III. Point 3 belongs to this category, which is the load speed located in the upward segment of the displacement curve. Corresponding to this point, the load acceleration yields larger maximum displacement, while the deceleration yields smaller.

(4) Category IV. Point 5 belongs to this category, which is the load speed located in the downward segment of the displacement curve. Corresponding to this point, the load acceleration yields smaller maximum displacement, while the deceleration yields larger.

The change of maximum displacement should increase with acceleration variation. Most of the data in Table 2.1 comply with this law, indicating the load-bridge resonance theory is valid for load with variable speed, while a few data in bold do not. These exceptions can be explained as follows.

(1) Due to the influence of speed incremental step, the calculated representative speeds yielding the peaks and valleys are not precise enough, so they are only the approximations of the real ones.
(2) When the load moves at variable speeds, the load position on the bridge yielding the maximum mid-span displacement is slightly different from that at constant speeds, and thus, the maximum displacement will be different.

It can be concluded that the maximum displacement of the bridge is associated with the initial speed and acceleration of the load, as well as the speed and position of the load corresponding to the maximum displacement. The conclusions above are confirmed by the analysis of the 3×32 m simply-supported bridge subjected to the moving WSM load, showing that

(1) When the load moves with different accelerations, the displacement time history curves of the bridge are almost the same, with difference less than 3% among their peak values. Therefore, the assumption of constant load speed is sufficient for usual analysis.
(2) When the load moves at a variable speed, the maximum mid-span displacement of the bridge is associated with the speed and position of the load arriving near the mid-span. The variation characteristics of maximum displacement versus load speed are in accordance with that when the load moves at a constant speed.

2.3 Resonance Analysis of a Simply-Supported Beam Subjected to Moving Loads

According to the fundamental theorems of structural dynamics, when a row of train vehicles travels over a railway bridge, the loading frequency (dependent on the train speed, bridge span, and composition of train vehicles) will change with the train speed and a resonant vibration will occur when the loading frequency coincides with the natural frequency of the bridge. The strong vibration induced by the resonance not only directly affects the working state and serviceability of the bridge, but also reduces the running safety of the train, diminishes the riding comfort of the passengers, and sometimes even destabilizes the ballasted track on the bridge. Therefore, it is necessary to develop methods to predict the resonant speeds of the running train and to assess the dynamic behavior of the bridge under resonance conditions.

In the past decades, researchers offered a lot of efforts to study the resonance problem of bridges under moving loads, such as by Matsuura (1976), Xia and Chen

(1992), Frýba (1999, 2001), Diana and Cheli (1989), Yang et al. (1997, 2004a, b), Yau and Yang (1999), Cheung et al. (1999), Li and Su (1999), Yau (2001), Savin (2001), Pesterev et al. (2003), Kwark et al. (2004), Xia et al. (2006, 2012), Ju and Lin (2003), Garinei and Risitano (2008), Hamidi and Danshjoo (2010), Michaltsos and Raftoyiannis (2010), Zambrano (2011), Rocha et al. (2012), Lee et al. (2012), Luu et al. (2012), and Lavado et al. (2014), and many of these models have been validated by field experiments (Liu et al. 2009; Xia and Zhang 2005; and Xia et al. 2012).

There are various factors associated with the resonance of the train-bridge system under moving loads, such as the periodic loading on the bridge by the regularly arranged wheel-axle loads due to vehicle gravity or centrifugal force, the periodic impact on the bridge caused by wheel scars, the periodic excitations induced by local track irregularities, the lateral periodic loading by hunting movement and centrifugal forces of train vehicles, the lateral moving load series caused by winds on car-bodies, and the periodical actions on moving vehicles by deflections of long bridge with identical multi-spans. The excitation frequencies by all the above factors are associated with the train speed. Consequently, investigation on the train-bridge resonance is significant in theory as well as in engineering practice.

2.3.1 Bridge Resonance Induced by a Moving Load Series

The resonance of train-bridge system is affected by the span, total length, lateral stiffness and vertical stiffness of the bridge, the compositions of the train, and the axle arrangements and natural frequencies of the vehicles. The general mechanism of bridge resonance induced by moving load series can be described as follows.

2.3.1.1 Fundamental Analysis Model

A simply-supported beam subjected to a train load is analyzed herein. The beam has a span L, a uniform mass $\bar{m}$, a bending stiffness EI, and a zero damping. The train consists of several identical cars with the full length l_v of each car, the rated distance l_c between the two bogies of the car, and the fixed wheelbase l_w between the two wheel-axles of the bogie, as shown in Fig. 2.16a. To explain the general principles and to facilitate the derivation, the train axle loads are simplified as N moving concentrated constant loads with identical interval d_v, as shown in Fig. 2.16b.

Suppose the load series travels on the beam from left to right at a uniform speed V, and the traveled distance of the first force is $x = Vt$. For the load series with identical intervals, there exists a time delay $\Delta t = d_v/V$ between any two successive forces. The motion equation for the beam acted on by such moving load series can be written as

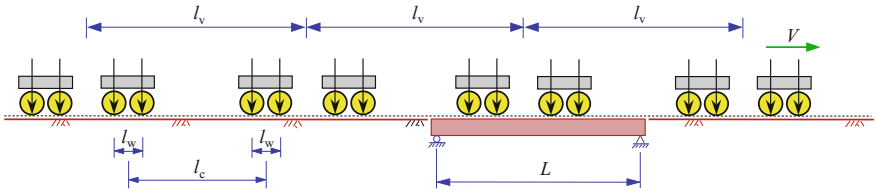

(a) Arrangement of wheel-axle loads of a train

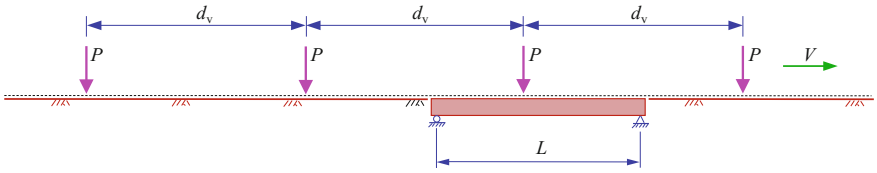

(b) Simplified moving load series

Fig. 2.16 Moving load series of a train on the bridge

$$EI\frac{\partial^4 y(x,t)}{\partial x^4}+\bar{m}\frac{\partial^2 y(x,t)}{\partial t^2}=\sum_{k=0}^{N-1}\delta\left[x-V(t-\frac{k\cdot d_v}{V})\right]P \tag{2.65}$$

It can be expressed in terms of the generalized coordinates as

$$\ddot{q}_n(t)+\omega_n^2 q_n(t)=\frac{2}{\bar{m}L}P\sum_{k=0}^{N-1}\sin\frac{n\pi V}{L}\left(t-\frac{k\cdot d_v}{V}\right) \tag{2.66}$$

Equation (2.66) is the motion equation of a SDOF system subjected to harmonic load series. The particular solution of Eq. (2.66) is

$$q(t)=\frac{2PL_b^3}{EI\pi^4}\frac{1}{1-\beta^2}\sum_{k=0}^{N-1}\left[\sin\bar{\omega}\left(t-\frac{k\cdot d_v}{V}\right)-\beta\sin\omega_1\left(t-\frac{k\cdot d_v}{V}\right)\right] \tag{2.67}$$

where $\bar{\omega}=\pi V/L$ is the exciting circular frequency of the moving load, and $\omega_1=\frac{\pi^2}{L^2}\sqrt{\frac{EI}{\bar{m}}}$ is the fundamental circular frequency of the beam. The displacement response of the beam where only the first mode is considered can thus be expressed as

$$y(x,t)=\frac{2PL_b^3}{EI\pi^4}\frac{1}{1-\beta^2}\sin\frac{\pi x}{L}\cdot\left[\sum_{k=0}^{N-1}\sin\bar{\omega}\left(t-\frac{k\cdot d_v}{V}\right)-\beta\sum_{k=0}^{N-1}\sin\omega_1\left(t-\frac{k\cdot d_v}{V}\right)\right] \tag{2.68}$$

where $\beta = \bar{\omega}/\omega_1$ is the ratio of exciting frequency to the fundamental frequency of the beam, and $1/(1-\beta^2)$ is the dynamic magnification factor.

The first term of the right-hand side of Eq. (2.68) represents the forced response of the beam due to the moving loads, while the second term represents the transient response due to its free vibration. According to their different mechanisms, the resonant responses of a simply-supported beam subjected to moving load series can be divided into two types.

2.3.1.2 Bridge Resonance Induced by Periodically Loading of Moving Load Series

First, the discussion is made for the second progression term of Eq. (2.68), to explain how the transient response in common sense may induce the resonance of the beam.

Before considering the second progression series, it is instructive to introduce the necessary transformation of triangular progression. For the sum of a finite triangular progression $\sin(a-ix)$, (i = 1, 2, …, m), it can be expressed as

$$\sum_{i=1}^{m} \sin(a-ix) = \sum_{i=1}^{m} [\sin a \, \cos ix - \cos a \, \sin ix] \tag{2.69}$$

The two terms of Eq. (2.69) can be further expressed as (Rade and Westergren 2010)

$$\begin{cases} \sum\limits_{i=1}^{m} \sin ix = \sin 0.5mx \cdot \sin 0.5(m+1)x \cdot \csc 0.5x \\ \sum\limits_{i=1}^{m} \cos ix = \sin 0.5mx \cdot \cos 0.5(m+1)x \cdot \csc 0.5x \end{cases} \tag{2.70}$$

Introducing them into Eq. (2.69) leads to

$$\sum_{i=1}^{m} \sin(a-ix) = \frac{\sin 0.5mx \cdot \sin[a-0.5(m+1)x]}{\sin 0.5x} \tag{2.71}$$

Now, let $i = k, m = N-1, x = \omega_1 d_v/V$, and $a = \omega_1 t$; the progression term of the transient response in Eq. (2.68) becomes as the form

$$\begin{aligned} \sum_{k=0}^{N-1} \sin \omega_1 \left(t - \frac{k \cdot d_v}{V} \right) &= \sin \omega_1 t + \sum_{k=1}^{N-1} \sin \omega_1 \left(t - \frac{k \cdot d_v}{V} \right) \\ &= \sin \omega_1 t + \frac{\sin\left[(N-1) \cdot \frac{\omega_1 d_v}{2V}\right] \cdot \sin\left[\omega_1 t - N \cdot \frac{\omega_1 d_v}{2V}\right]}{\sin \frac{\omega_1 d_v}{2V}} \end{aligned} \tag{2.72}$$

For $\frac{\omega_1 d_v}{2V} = \pm i\pi$, the second term of Eq. (2.72) becomes an indeterminate form 0/0, but when the L'Hospital's rule is applied, the limit solution is found to be

$$\lim_{\frac{\omega_1 d_v}{2V} \to \pm i\pi} \frac{\sin\left[(N-1)\cdot\frac{\omega_1 d_v}{2V}\right]\cdot \sin\left[\omega_1 t - N\cdot\frac{\omega_1 d_v}{2V}\right]}{\sin\frac{\omega_1 d_v}{2V}} = (N-1)\sin\omega_1\left[t - N\cdot\frac{d_v}{2V}\right] \tag{2.73}$$

Obviously, the extreme condition with physical significance for Eq. (2.73) is

$$\frac{\omega_1 d_v}{2V} = i\pi \quad (i = 1, 2, 3, \cdots) \tag{2.74}$$

Substituting this condition into Eq. (2.71), the limit value of the transient response term in Eq. (2.67) is obtained as

$$\sum_{k=0}^{N-1} \sin\omega_1\left(t - \frac{k\cdot d_v}{V}\right)\Big|_{\frac{\omega_1 d_v}{2V} = i\pi} = N\sin\omega_1 t \tag{2.75}$$

It can be seen that each force in the moving load series may induce the transient response of the structure, and the successive forces form a series of periodical excitations. The response of the structure will be successively amplified with the increase of N, the number of forces traveling through the beam, resulting in the structural resonance.

Similar results can be obtained for higher modes of the bridge. Considering all of these modes and letting $\omega_n = 2\pi f_{bn}$, the resonant condition of the bridge under a moving load series can be derived from Eq. (2.72) as

$$V_{br} = \frac{3.6\cdot f_{bn}\cdot d_v}{i} \quad (n = 1, 2, 3, \cdots)(i = 1, 2, 3, \cdots) \tag{2.76}$$

where V_{br} is the resonant train speed (km/h); f_{bn} is the nth vertical or lateral natural frequency of the bridge (Hz); d_v is the intervals of the moving loads (m); and the multiplicator i = 1, 2, 3 is determined by the extreme condition Eq. (2.74).

Equation (2.76) indicates that when a train moves on the bridge at speed V, the regularly arranged wheel-axle loads may produce periodical dynamic actions on the bridge with the loading period d_v/V. The bridge resonance occurs when the loading period is close to the nth natural vibration period of the bridge or its i times. A series of resonant responses related to different bridge natural frequencies may occur corresponding to different train speeds. The appearance of this phenomenon is determined by the time of the load traveling through the distance d_v. Equation (2.76) is called as ***the first resonant condition*** of simply-supported bridge. Detailed illustration on the physical meaning of the bridge resonance induced by the moving load series will be presented in Sect. 2.4.3.

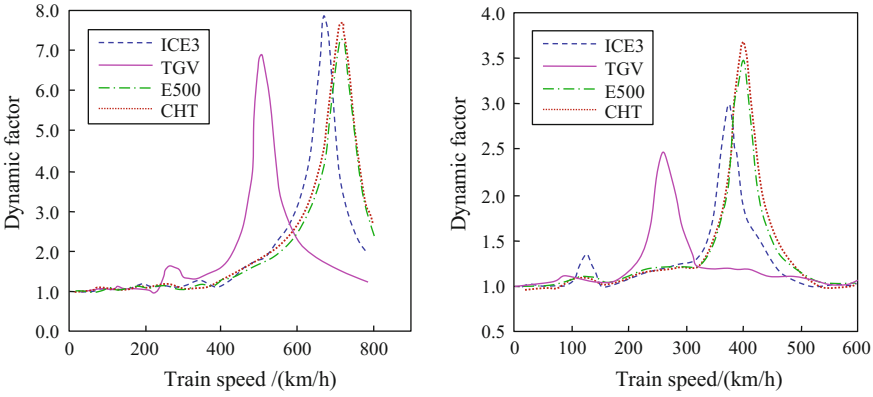

(a) L=20m (b) L=32m

Fig. 2.17 Dynamic factors of simply-supported beams versus train speed

During the dynamic analysis of the bridges on the Beijing-Shanghai HSR, the dynamic interaction model of train-bridge system was used to study the resonant responses induced by various high-speed trains, such as Germany ICE3, France TGV, Japan E500, and China CHT. Shown in Fig. 2.17 are the simulated distribution curves of dynamic factors versus train speed for the PC box-beams with 20 and 32 m spans, where the dynamic factor is defined as the ratio of the maximum dynamic to the maximum static deflection of the beam under the same loading.

It is given that the natural frequencies of the 20 m and 32 m PC box-beams are 7.73 Hz and 4.23 Hz, respectively. By using Eq. (2.76), the corresponding resonant train speeds can be estimated as 520 km/h and 284.8 km/h for TGV whose average car length is l_v = 18.7 m, and 285 km/h and 400 km/h for ICE3, E500, and CHT whose average car lengths are all $l_v \approx 26$ m. In this example, the calculation is based on $d_v = l_v$; namely, the full length of vehicle is taken as the load interval, where the four axle loads of the rear bogie at the previous car and the front bogie at the following car are combined as one concentrated load. The resonant train speeds estimated by Eq. (2.76) are in good accordance with the critical train speeds from the simulated results, as compared in Fig. 2.17.

Equation (2.76) can also be used to analyze the lateral response of bridge under the first resonant condition. The lateral resonance analysis has special significance for bridges with high piers under a moving load series induced by centrifugal forces or lateral wind pressures. Since the lateral frequency of the bridge system is usually smaller than the vertical frequency, the critical train speed for lateral resonance is also lower.

A simply-supported steel truss with the span of 48 m is analyzed as an example. The moving load series are the lateral axle loads induced by wind pressures acting on car-bodies.

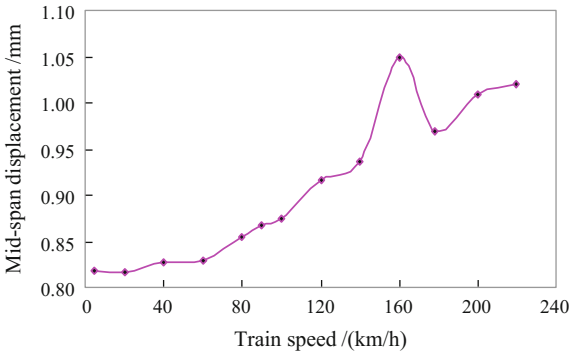

Fig. 2.18 Lateral displacements of steel truss versus train speed

The lateral natural frequency of the truss is 1.86 Hz. The train concerned is composed of one locomotive followed by 18 passenger cars. The full length of each car is 26.57 m. The resonant train speed for the first resonant condition estimated by Eq. (2.76) is

$$i = 1 : V_{\mathrm{br}1} = \frac{1.86 \times 26.57}{1} \times 3.6 \approx 178\,\mathrm{km/h}$$
$$i = 2 : V_{\mathrm{br}2} = \frac{1.86 \times 26.57}{2} \times 3.6 \approx 89\,\mathrm{km/h}$$
$$i = 3 : V_{\mathrm{br}3} = \frac{1.86 \times 26.57}{3} \times 3.6 \approx 60\,\mathrm{km/h}$$

According to the predicted results, the dynamic responses of the truss under various train speeds are analyzed by the whole history simulations of train-bridge system, with the calculation train speeds in the range of 5–220 km/h. Figure 2.18 shows the distribution curve of lateral mid-span displacements of the truss versus train speed.

It can be found that during the train passage, an obvious peak appears at the speed of 160 km/h, and two small peaks appear at the speeds of 80 and 40 km/h, showing significant harmonic resonances of the first order. Considering that the natural frequency of the bridge will decrease when loaded by the train, the estimated results obtained from Eq. (2.76) are in accordance with those from the whole history simulations of train-bridge system.

2.3.1.3 Bridge Resonance Induced by Loading Rate of a Moving Load Series

As for the first progression term of Eq. (2.68) which represents the forced response of the bridge, the solution is almost the same as the second term except that it misses the multiplicator β and uses $\bar{\omega}$ instead of ω_1; thus, an extreme condition similar to Eq. (2.74) can be directly written as

$$\frac{\bar{\omega} d_{\mathrm{v}}}{2V} = i\pi \, (i = 1, 2, 3, \ldots) \tag{2.77}$$

Substituting $\bar{\omega} = \pi V/L$ into Eq. (2.77), the train speed V in the numerator is counteracted with that in the denominator and thus results in the extreme condition

$$d_{\mathrm{v}} = 2iL \quad (i = 1, 2, 3, \ldots) \tag{2.78}$$

The limit value of the steady-state response progression can be obtained by using this extreme condition

$$\sum_{k=0}^{N-1} \sin \bar{\omega} \left(t - \frac{k \cdot d_{\mathrm{v}}}{V} \right) \Big|_{\frac{\bar{\omega} d_{\mathrm{v}}}{2V} = i\pi} = N \sin \bar{\omega} t \tag{2.79}$$

There is no train speed V expressed in Eq. (2.78); namely, no resonant train speed exists. Equations (2.78) and (2.79) show that when the interval of loads equals to $2i$ times of the bridge span, i.e., the half-wavelength formed by the beam deflection, the successive increase of the number of passing wheel-axles may gradually enlarge the bridge response. However, since the minimum axle intervals of real vehicles are much smaller than two times of the bridge span length, and the actual arrangement of train wheel-axles is never identical, this solution is only of mathematical significance. Therefore, the resonant train speed cannot be derived in this way.

In fact, the second resonance of the simply-supported beam under moving train loads can be directly determined from Eq. (2.68) by the dynamic magnification factor $1/(1 - \beta^2)$. For the nth bridge modes, $\bar{\omega}_n = n\pi V/L$ is the nth exciting frequency. Obviously, when the frequency ratio β_n is equal to 1, i.e., $\omega_n = \bar{\omega}_n$, the dynamic magnification factor $1/(1 - \beta_n^2)$ will become infinitive. At this time, the nth resonant vibration of the bridge is excited. For the simply-supported beam under moving loads, the nth natural frequency of the beam $\omega_n = 2\pi f_{\mathrm{b}n}$, and thus, the resonant train speed V_{br} can be described as

$$V_{\mathrm{br}} = \frac{7.2 \cdot f_{\mathrm{b}n} \cdot L}{n} \quad (n = 1, 2, 3, \ldots) \tag{2.80}$$

where V_{br} is the resonant train speed (km/h); $f_{\mathrm{b}n}$ is the nth vertical or lateral natural frequency of the bridge (Hz); and L_{b} is the span of the bridge (m).

Equation (2.80) indicates that bridge resonance occurs when the traveling time of the train through the bridge equals to $0.5n$ times the nth vibration period of the bridge. The appearance of this phenomenon is determined by the loading rate of moving loads related to the bridge span. Equation (2.80) is called as ***the second resonant condition*** of simply-supported bridge, in which V_{br} is nothing less than the resonant speed derived at $\alpha = k$ in Sect. 2.1.

The resonant train speed calculated from Eq. (2.80) is rather high. For instance, the lowest natural frequencies for the simply-supported beams with moderate or small spans are 80/L and 120/L, respectively, given in the Chinese codes *Interim Provisions on Design of New 200* km/h *Passenger-cum-freight Railways* (TJS 2005-285 2005a, b) and the *Interim Provisions on Design of Beijing-Shanghai HSR* (TJS 2003-13 2003), by which the resonant train speeds can be estimated by Eq. (2.80) as 576 and 864 km/h. These values are far higher than the current train speeds in operation. Thus, currently, the vertical resonance of a simply-supported beam is analyzed mainly based on the first resonant condition, while for trains with higher speed, e.g., a maglev train, the second resonant condition is of certain significance in resonance analysis.

When the train is running on the bridge, the centrifugal forces or the lateral wind pressures on the car-bodies will be transferred via wheel-sets to the bridge structure. These actions can be represented by a series of lateral moving loads. When the excitation frequency of the moving load series is equal or close to the bridge natural frequency, the second resonant response will occur. The corresponding critical train speed V_{br} can be estimated through Eq. (2.80). The relationship between the bridge lateral resonant response induced by a moving load series due to mean wind pressure on the vehicle and critical train speeds is illustrated through a realistic example.

For bridges with high piers often encountered in engineering, owing to their low natural frequencies, the analysis on both the first and the second lateral resonances is of significance. Since a pier cannot directly support train loads, a bridge composed of two 32 m simply-supported beams and a 56 m high pier is analyzed as an example. The moving load series are formed by the same lateral wind loads as in the previous example. Modal analysis shows that the first three modes of the bridge are dominated by the lateral vibrations of the pier. With respect to the bridge lateral frequencies 0.95, 2.52, and 5.02 Hz, the resonant train speeds estimated by the first resonant condition Eq. (2.74) include

$$\begin{aligned}
f_{\mathrm{b1}} = 0.95\,\mathrm{Hz}: &\quad V_{\mathrm{br1}} = 91\,\mathrm{km/h}, &\quad V_{\mathrm{br2}} = 46\,\mathrm{km/h}, &\quad V_{\mathrm{br3}} = 31\,\mathrm{km/h}\\
f_{\mathrm{b2}} = 2.52\,\mathrm{Hz}: &\quad V_{\mathrm{br1}} = 240\,\mathrm{km/h}, &\quad V_{\mathrm{br2}} = 120\,\mathrm{km/h}, &\quad V_{\mathrm{br3}} = 81\,\mathrm{km/h}\\
f_{\mathrm{b3}} = 5.02\,\mathrm{Hz}: &\quad V_{\mathrm{br1}} = 481\,\mathrm{km/h}, &\quad V_{\mathrm{br2}} = 240\,\mathrm{km/h}, &\quad V_{\mathrm{br3}} = 161\,\mathrm{km/h}
\end{aligned}$$

For the 2×32 m bridge, the lateral loading length to the pier is L = 64 m, so the possible resonant train speeds estimated from the second resonant condition Eq. (2.80) include

$$\begin{aligned}
n = 1: V_{\mathrm{br1}} &= \frac{7.2 \times 0.95 \times 64}{1} \approx 438\,\mathrm{km/h}\\
n = 2: V_{\mathrm{br2}} &= \frac{7.2 \times 2.52 \times 64}{2} \approx 581\,\mathrm{km/h}\\
n = 3: V_{\mathrm{br3}} &= \frac{7.2 \times 5.02 \times 64}{3} \approx 771\,\mathrm{km/h}
\end{aligned}$$

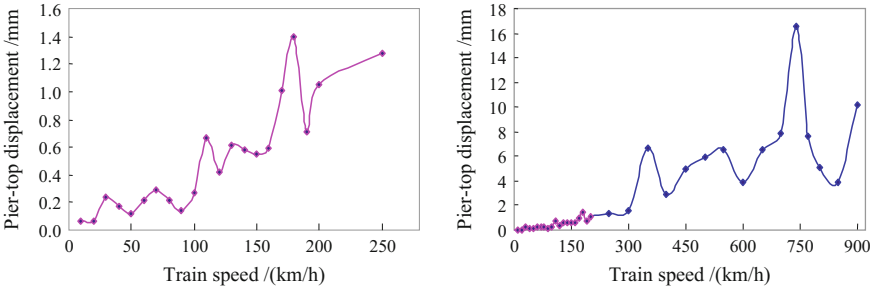

Fig. 2.19 Lateral displacement of the pier-top versus train speed

The dynamic responses of the bridge under various train speeds are analyzed by the whole history simulations of train-bridge system, with the calculation train speeds in the range of 10–900 km/h. Figure 2.19 shows the distribution curves of lateral displacements of the pier-top versus train speed.

The curves show that the lateral resonance of the pier is obvious: The peak values of lateral displacement are found in the positions slightly lower than the estimated critical velocities by the first resonant condition, and also the peak displacements at 380 and 740 km/h, which are close to the corresponding resonant train speeds estimated by the second resonant condition. Considering the natural frequency of bridge will decrease when loaded by the train, the estimated results by Eqs. (2.76) and (2.80) are in accordance with those from the whole history simulations of train-bridge system.

Furthermore, one can estimate the responses of the bridge under vehicle centrifugal forces. As moving load series, the vehicle centrifugal forces have the same mechanism to induce the lateral vibration of the bridge as the mean wind pressures acting on the car-bodies. Thus, the calculated curves in Fig. 2.19 can also be used for estimating centrifugal forces. According to the Chinese code *Fundamental Code for Design on Railway Bridge and Culvert* (TB10002.1-2005 2005), $\bar{m}$ force can be 15% of the static load of vehicles, which is about 2.5 times of the vehicle design wind load. Therefore, when considering the vehicle centrifugal forces, much greater pier-top displacements will be excited than those shown in Fig. 2.19.

2.3.1.4 Bridge Resonance Owing to the Sway Forces of Train Vehicles

The third bridge resonance is induced by the periodical actions of lateral moving load series on the bridge owing to the sway forces of train vehicles. The sway forces of vehicles may be excited by track irregularities and wheel hunting movements. The resonant train speed in this case can be determined by

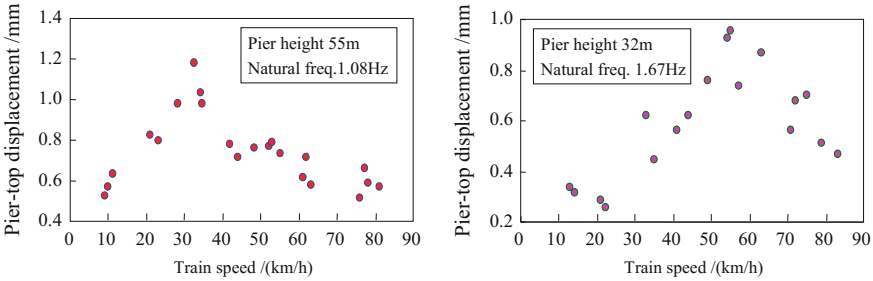

Fig. 2.20 Lateral displacements of high piers versus train speed

$$V_{\mathrm{br}} = \frac{3.6 \cdot f_{\mathrm{b}n} \cdot L_{\mathrm{s}}}{i} (n = 1, 2, 3, \cdots; i = 1, 2, 3, \cdots) \tag{2.81}$$

where $f_{\mathrm{b}n}$ is the nth vertical or lateral natural frequency of the bridge (Hz); L_{s} is the dominant wavelength of track irregularities or wheel hunting movement. The multiplicators i = 1, 2, 3,… show that when the dominant frequency of track irregularities or wheel hunting movement equals to the nth natural frequency or higher harmonic frequencies, the resonance of the bridge occurs. This is called ***the third resonant condition*** of bridge.

Although both track irregularities and wheel hunting movement are of random properties, Eq. (2.81) can still be used to estimate the lateral resonance of bridge induced by their dominant wavelengths. A good example is presented in Fig. 2.20, the distributions of the lateral displacements of two high piers versus train speed. The data in the figure were measured in the field experiments at two real bridges on the Chengdu-Kunming Railway in China. One can find peak values appearing at certain train speeds, which are in good accordance with the estimated resonant train speeds of 33 km/h and 51.1 km/h, respectively. The estimated resonant train speeds are calculated by Eq. (2.81), using the hunting wavelength L_{s} = 8.5 m for wheels with worn threads, the given pier heights H = 55 m and 32 m, and the corresponding bridge frequencies f = 1.08 Hz and 1.67 Hz, respectively.

2.3.1.5 Application Scopes of Resonance Conditions

Based on the analysis above, the resonant vibrations of bridges induced by moving trains have been classified into three mechanisms. The first is related to the intervals of the moving load series, which form the periodically loading on the bridge. The second is induced by the loading rate, i.e., the relative moving speed of the load series to the bridge. The third is owing to the swing forces of the train vehicles excited by track irregularities and wheel hunting movement.

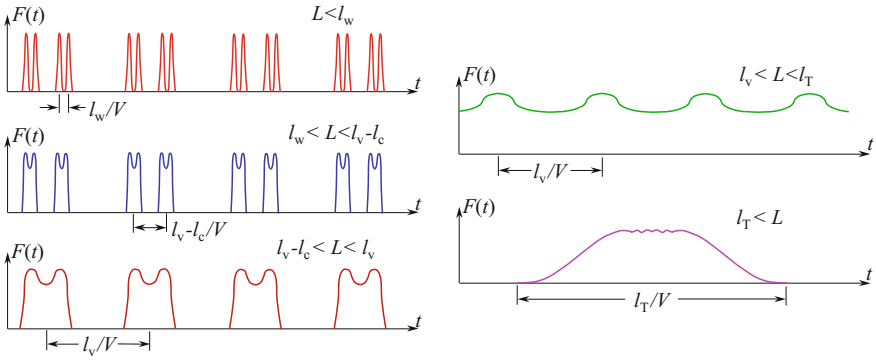

Fig. 2.21 Time histories of load series moving on bridge

In the above resonant conditions, the axle loads of the train vehicles are assumed to be in equidistance. While in reality, there exist several axle intervals in a train: the full length l_v of a car, the rated center-to-center distance l_c between two bogies of a car, the fixed wheelbase l_w between two wheel-sets of a bogie, and the different compositions of these distances. According to the relative lengths between the beam span or the bridge length and the above loading intervals, when Eq. (2.76) is used to analyze the first resonance induced by moving trains, the application scopes can be further discussed as follows (ref. Figs. 2.16 and 2.21):

(1) $L<l_w$: When the bridge length L is shorter than the fixed wheelbase l_w of a bogie, there can be only one wheel-set at any moment on the bridge, with the shortest excitation period $l_w = V$ and some other longer periods as $(l_v - l_c)/V$ and l_v/V. However, it is only an extreme situation in theory, for there exists no such short bridge in reality.

(2) $l_w < L < l_v - l_c$: When the bridge length L is longer than the fixed wheelbase l_w of a bogie but shorter than the distance $l_v - l_c$ between the rear bogie of the previous car and the front bogie of the following car, there can still be only one wheel-set at any moment on the bridge, with the main excitation period $(l_v - l_c)/V$ and some longer periods as l_v/V, while the shorter period l_w/V is not obvious. This situation may occur for the bridges with very short spans.

(3) $l_v - l_c < L < l_v$: When the bridge length L is longer than the distance $l_v - l_c$ between the rear bogie of the previous car and the front bogie of the following car, but shorter than the full length l_v of the car, there can be two wheel-sets simultaneously on the bridge, with the main excitation period l_v/V, while the shorter periods as l_w/V and $(l_v - l_c)/V$ are not obvious. Since the full lengths are about 25 m for passenger car and 15 m for freight car, this situation may occur for common bridges with small spans.

(4) $l_v < L < l_T$: When the bridge length L is longer than the full length l_v of a car but shorter than the total length l_T of the whole train, there can be more than one cars and two wheel-sets simultaneously on the bridge, neither of the above

excitation periods as l_w/V, $(l_v - l_c)/V$ nor l_v/V is obvious. This situation may occur for common bridges with moderate spans or for lateral resonance analysis of the bridge as a whole.

(5) $l_T < L$: When the bridge length L is longer than the total length l_T of a train, there can be several cars with many wheel-sets simultaneously on the bridge; thus, the load series cannot form periodical loading to the bridge system. This situation may occur for long-span bridges, or for lateral resonance analysis of the bridge as a whole. However, the resonant conditions proposed in this section cannot be directly used to analyze the resonant conditions for long-span bridges, because the whole course of a train traveling over the bridge longer than the total length of the train is equivalent to a half-loading period, and thus, no harmonic load forms. Therefore, Eqs. (2.76) and (2.80) cannot be directly used to estimate the resonant train speeds. As for the third resonant condition where the bridge resonance is excited by track irregularities or wheel hunting, no obvious resonance can be observed for long-span bridges because of the counteractions between the forces from the wheel-sets moving with different phases.

Thus, it can be seen that when using the above equations to analyze the train-induced resonance of the bridge, the loading intervals can be the full length l_v of a car, the rated center-to-center distance l_c between two bogies of a car, the fixed wheelbase l_w of a bogie, and the various compositions of these distances. While for a row of train vehicles, the arrangement of the axle loads is not in equidistance, and neither equal are the values of all axle forces which are affected by the bridge damping, track irregularities, and other complicated factors. Accordingly, a series of resonant vibrations may be excited with different response levels when the train moving at various speeds on the bridge, and a series of corresponding resonant train speeds could be found. Therefore, the precise resonance analysis usually depends on the simulation calculations of the train-bridge dynamic interaction system according to the real conditions of train composition, wheel arrangement, and vehicle loads.

2.3.2 *Resonance Analysis of Train Vehicles*

As a train runs on a long bridge at the speed V, the periodical actions on the vehicle can be excited by successive deflections of the bridge that consists of a series of identical spans (see Fig. 2.22), which can be considered as periodic track irregularities with frequency V/L_b. Resonance occurs to the vehicle when this loading frequency coincides with the natural frequency of the vehicle, and the dynamic responses of the vehicle will be greatly amplified. The critical train speed in this case can be written as

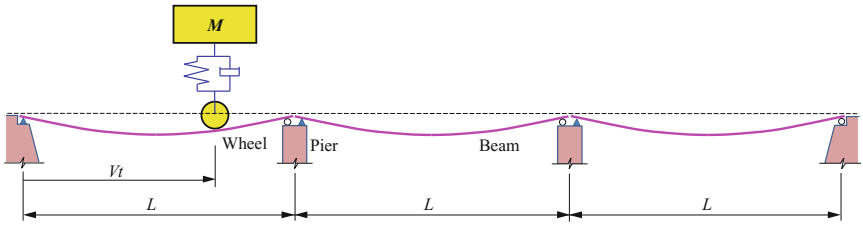

Fig. 2.22 Vehicle vibration induced by bridge deflections

$$V_{\mathrm{vr}} = 3.6 \cdot f_{\mathrm{v}} \cdot L \tag{2.82}$$

where V_{vr} is the critical train speed (km/h); f_{v} is the natural vertical frequency of vehicle (Hz); and L_{b} is the span length of bridge (m).

The excitation of bridge deflections on the vehicle is equivalent to a wheel-spring-mass system on the ground in harmonic motions. The transmissibility between the amplitudes of the mass and the deflection of the beam can be estimated as (Clough and Penzien 2003)

$$\mathrm{TR} = \sqrt{\frac{1 + (2\xi\beta)^2}{(1 - \beta^2)^2 + (2\xi\beta)^2}} \tag{2.83}$$

For a half-vehicle model with sprung-mass M = 24 t, equivalent spring stiffness k = 800 kN/m, and damping ratio ξ = 0.2, the natural frequency is calculated as 0.92 Hz. At the critical train speed, i.e., β = 1, the transmissibility can be calculated as TR = 2.69. It means when the deflection of the bridge is 2 mm, the amplitude of the vehicle will be as large as 5.38 mm. Moreover, the resonance of vehicles will in turn enlarge the dynamic impact on the bridge.

The fundamental vertical natural frequencies of train vehicles are usually between 0.8 and 1.5 Hz. For the railway bridges with 20 m $\sim$ 40 m spans, the corresponding critical train speeds could thus be estimated as V_{vr} = 57 km/h $\sim$ 216 km/h. To prevent or to suppress vehicle resonance due to bridge deflections, therefore, attentions should be paid in design to avoid long series of identical spans, or to reduce the deflection by strengthening structural stiffness.

2.4 Vibration Suppression and Cancellation Analysis of Train-Bridge System

In studying the train-bridge resonance, Yang et al. (1997) found that resonance of the bridge may not occur at certain ratios between span length and characteristic load distance. Savin (2001) discovered that when a single load passing a

simply-supported bridge at different speeds, the amplitude of free vibration changes and declines to null at some speeds. This interesting finding interprets the vibration cancellation effect; namely, when a single load passes the bridge at a cancellation speed, the residual free vibration of the bridge will be null after the load leaves it.

Unlike the resonance effect that enlarges the bridge response, the cancellation effect may suppress the vibration of the bridge, which is favorable for train running safety and bridge service. Therefore, an insight investigation into the cancellation effect is of important significance, and some further investigations have been done, such as those by Yau et al. (2001), Pesterev et al. (2003), Yang et al. (2004a, b), Museros et al. (2013), and Xia et al. (2014).

In this section, vibrations of the simply-supported beam under a moving single force, equidistant load series, and train loads are theoretically analyzed, in terms of bridge free vibration after each load leaving the bridge. By analysis of the vibration responses, the occurrence conditions of resonance and two types of vibration cancellation effects on the simply-supported beam are derived for any mode. Additionally, the influence of vibration cancellation on resonance is investigated, and conditions for resonance disappearance are obtained. The resonance and cancellation mechanisms and characteristics of bridge response are illustrated through numerical case study.

2.4.1 Resonance and Cancellation of Simply-Supported Beam Under Moving Equidistant Load Series

2.4.1.1 Analysis Model

A simply-supported beam bridge subjected to a train load is analyzed herein, using the same model as shown in Fig. 2.16. The train is simplified as a series of moving loads with identical interval, each force P represents a concentrated constant car load, and the interval l_v denotes the full length of a car. Thus, a train composed of N_v cars can be considered as N_v moving forces, numbered as P_k ($k = 1, 2, 3, \ldots N_v$). If the initial time is defined as the moment when the first load gets onto the bridge, the time of the kth load entering the bridge can be expressed as

$$t_k = (k-1)l_v/V \tag{2.84}$$

where V is the moving speed of the train.

2.4.1.2 Analytical Solution for Bridge Vibration Response

Ignoring the damping effect, the motion equation of the bridge under moving equidistant loads can be expressed as

$$\bar{m}\frac{\partial^2 y(x,t)}{\partial t^2}+EI\frac{\partial^4 y(x,t)}{\partial x^4}=\sum_{k=1}^{N_v}P\delta[x-V(t-t_k)] \tag{2.85}$$

where $\bar{m}$ and EI are, respectively, the mass per unit length and the bending stiffness of the bridge; $y(x, t)$ is the displacement of the bridge at position x and time t; and δ is the Dirac delta function.

Equation (2.85) is a partial differential equation, whose initial and boundary conditions can be expressed as

$$\begin{cases} y(x,0)=\dot{y}(x,0)=0 \\ y(0,t)=y(L,t)=0 \\ EIy''(0,t)=EIy''(L,t)=0 \end{cases} \tag{2.86}$$

For a simply-supported beam, Eq. (2.85) can be solved through the modal decomposition method. The displacement of the beam can be expressed by $y(x,t)=\sum_{n=1}^{\infty}q_n(t)\sin\frac{n\pi x}{L}$, namely the product of generalized coordinates $q(t)$ and mode shapes. Thus, Eq. (2.85) can be rewritten in terms of generalized coordinates as

$$\ddot{q}_n(t)+\omega_n^2 q_n(t)=\frac{2P}{\bar{m}L}\sum_{k=1}^{N_v}\sin\left(\frac{n\pi V(t-t_k)}{L}\right) \tag{2.87}$$

where $\omega_n=\left(\frac{n\pi}{L}\right)^2\sqrt{\frac{EI}{\bar{m}}}$ is the nth circular frequency of the bridge.

Equation (2.87) is the motion equation of the simply-supported beam under a moving load series. Its particular solution is ($\beta_n \neq 1$)

$$y(x,t)=\frac{2P}{\bar{m}L}\sum_{n=1}^{\infty}\left\{\sin\left(\frac{n\pi x}{L}\right)\frac{1}{\omega_n^2(1-\beta_n^2)}\sum_{k=1}^{N_v}[\sin\bar{\omega}_n(t-t_k)-\beta_n\sin\omega_n(t-t_k)]\right\} \tag{2.88}$$

where $\bar{\omega}_n = n\pi V/L$ is the exciting frequency; $\beta_n = \bar{\omega}_n/\omega_n$ is the ratio of the exciting frequency of moving loads to the natural frequency of bridge, which can be expressed in terms of speed parameter α as $\beta_n = \alpha/n$. The case $\beta_n = 1$ corresponds to the second resonant condition, which has been discussed in Sects. 2.1 and 2.3, and is not described again herein.

Considering the case when the first (N−1) (N = 1, 2, 3, …, N_v) forces have left, and the Nth force is on the bridge, the displacement response of the bridge can be expressed by the following equation

$$y(x,t) = \frac{2P}{\bar{m}L}\sum_{n=1}^{\infty}\sin\left(\frac{n\pi x}{L}\right)\frac{1}{\omega_n^2(1-\beta_n^2)}Q_N(V,t) \tag{2.89}$$

where

$$\begin{aligned} Q_N(V,t) = {} & [\sin\bar{\omega}_n(t-t_N) - \beta_n \sin\omega_n(t-t_N)] \\ & - \beta_n \sum_{k=1}^{N-1}\left[\sin\omega_n(t-t_k) + (-1)^{n-1}\sin\omega_n\left(t-t_k-\frac{L}{V}\right)\right] \end{aligned} \tag{2.90}$$

The first term of $Q_N(V, t)$ represents steady and transient responses induced by the Nth force moving on the bridge. The second term is associated with the total residual responses (free vibration) induced by the first ($N-1$) forces that have left the bridge, which is derived from Eq. (2.88) as follows:

During $t_k \le t \le t_k + L/V$, the kth force is on the bridge, and the forced vibration response of the bridge induced by it can be written as

$$y_k(x,t) = \frac{2P}{\bar{m}L}\sum_{n=1}^{\infty}\sin\left(\frac{n\pi x}{L}\right)\frac{1}{\omega_n^2(1-\beta_n^2)}[\sin\bar{\omega}_n(t-t_k) - \beta_n\sin\omega_n(t-t_k)] \tag{2.91}$$

During $t > t_k + L/V$, the kth load has left the bridge, and the free vibration response of the bridge induced by it can be expressed as

$$\begin{aligned} y_k(x,t) = {} & \sum_{n=1}^{\infty} y_k^n(x, t_k + L/V)\cos\omega_n(t - t_k - L/V) \\ & + \sum_{n=1}^{\infty}\frac{\dot{y}_k^n(x, t_k + L/V)}{\omega_n}\sin\omega_n(t - t_k - L/V) \end{aligned} \tag{2.92}$$

where $y_k^n(x, t_k + L/V)$ and $\dot{y}_k^n(x, t_k + L/V)$ are, respectively, displacement and velocity of the nth mode at $t = t_k + L/V$, which are the initial conditions of the free vibration and can be derived from Eq. (2.91).

Substituting $y_k^n(x, t_k + L/V)$ and $\dot{y}_k^n(x, t_k + L/V)$ into Eq. (2.92), the total residual response of the bridge induced by the first $N-1$ forces can be expressed as

$$y_k(x,t) = -\frac{2P}{\bar{m}L}\sum_{n=1}^{\infty}\sin\left(\frac{n\pi x}{L}\right)\frac{1}{\omega_n^2(1-\beta_n^2)}\beta_n\sum_{k=1}^{N-1}\left[\sin\omega_n(t-t_k) + (-1)^{n-1}\sin\omega_n(t-t_k-L/V)\right] \tag{2.93}$$

From Eq. (2.93), the second term in the $Q_N(V, t)$ can be extracted. By applying the trigonometric transformation, Eq. (2.90) can be expressed as

$$Q_N(V,t) = [\sin\bar{\omega}_n(t-t_N) - \beta_n \sin\omega_n(t-t_N)] - 2\beta_n \sum_{k=1}^{N-1}\left[\cos\frac{\omega_n L}{2V}\sin\omega_n\left(t-t_k-\frac{L}{2V}\right)\right] \quad (n=1,3,5,\ldots) \tag{2.94a}$$

$$Q_N(V,t) = [\sin\bar{\omega}_n(t-t_N) - \beta_n \sin\omega_n(t-t_N)] - 2\beta_n \sum_{k=1}^{N-1}\left[\sin\frac{\omega_n L}{2V}\cos\omega_n\left(t-t_k-\frac{L}{2V}\right)\right] \quad (n=2,4,6,\ldots) \tag{2.94b}$$

It is not easy to observe the significant physical meanings of this equation. Therefore, by introducing Eqs. (2.84) and (2.70) into Eq. (2.94a, 2.94b), a more interesting expression for $Q_N(V,t)$ can be obtained as

$$Q_N(V,t) = [\sin\bar{\omega}_n(t-t_N) - \beta_n \sin\omega_n(t-t_N)] - 2\beta_n \cos\frac{\omega_n L}{2V}\left\{\sin\omega_n\left(t-\frac{L}{2V}-\frac{t_{N-1}}{2}\right)\frac{\sin(N-1)\frac{\omega_n L_v}{2V}}{\sin\frac{\omega_n L_v}{2V}}\right\} \quad (n=1,3,5,\ldots) \tag{2.95a}$$

$$Q_N(V,t) = [\sin\bar{\omega}_n(t-t_N) - \beta_n \sin\omega_n(t-t_N)] - 2\beta_n \sin\frac{\omega_n L}{2V}\left\{\cos\omega_n\left(t-\frac{L}{2V}-\frac{t_{N-1}}{2}\right)\frac{\sin(N-1)\frac{\omega_n L_v}{2V}}{\sin\frac{\omega_n L_v}{2V}}\right\} \quad (n=2,4,6,\ldots) \tag{2.95b}$$

2.4.1.3 Resonance and Cancellation

It is observed from Eq. (2.95a, 2.95b) that the residual free vibration in terms of generalized coordinates for the bridge induced by the first ($N-1$) forces can be expressed by a sinusoidal function (for odd-order modes) or a cosine function (for even-order modes).

For $\sin(\omega_n L_v/2V) = i\pi$, Eq. (2.95a, 2.95b) becomes an indeterminate form 0/0; however, when the L'Hospital's rule is applied, the limit solution is found to be

$$Q_N(V,t) = [\sin\bar{\omega}_n(t-t_N) - \beta_n \sin\omega_n(t-t_N)] - 2(N-1)\beta_n \cos\left(\frac{\omega_n L}{2V}\right)\sin\omega_n\left(t-\frac{L}{2V}\right) \quad (n=1,3,5,\ldots) \tag{2.96a}$$

$$Q_N(V,t) = [\sin\bar{\omega}_n(t-t_N) - \beta_n \sin\omega_n(t-t_N)] - 2(N-1)\beta_n \sin\left(\frac{\omega_n L}{2V}\right)\cos\omega_n\left(t-\frac{L}{2V}\right) \quad (n=2,4,6,\ldots) \tag{2.96b}$$

It can be seen from Eq. (2.96a, 2.96b) that the displacement of bridge will be successively amplified with the increase of the number N of forces traveling on the bridge. Therefore, by using the extreme condition $\omega_n L_v/2V = i\pi$, the resonant speed V_{res} (km/h) for the bridge under the moving load series can be expressed as

$$V_{res} = \frac{3.6 f_n L_v}{i} \quad (i=1,2,3,\cdots) \tag{2.97}$$

where f_n is the nth-order natural frequency of the bridge (Hz). Equation (2.97) has been defined as the first resonant condition in Sect. 2.3, where more details on the bridge resonance induced by the moving load series can be found.

When $\cos(\omega_n L/2V) = 0$ or $\sin(\omega_n L/2V) = 0$, the second term of $Q_N(V, t)$ in Eq. (2.94a, 2.94b) becomes zero and only the first term is left

$$Q_N(V,t) = [\sin\bar{\omega}_n(t-t_N) - \beta_n \sin\omega_n(t-t_N)] \tag{2.98}$$

In this case, the total residual response (free vibration) of the bridge excited by the first ($N-1$) forces is equal to null, while the vibration is determined only by the Nth force acting on the bridge. This phenomenon is herein defined as ***the first cancellation effect of vibration*** with the following conditions

$$\frac{\omega_n L}{2V} = i\pi - \frac{\pi}{2} \quad (n=1,\ 3,\ 5,\ldots;\ i=1,\ 2,\ 3,\ldots) \tag{2.99a}$$

$$\frac{\omega_n L}{2V} = i\pi \quad (n=2,4,6,\cdots;i=1,2,3,\ldots) \tag{2.99b}$$

It can be observed from Eq. (2.90) that when Eq. (2.99a, 2.99b) is satisfied, there is a $(2i\text{-}1)\pi$ or a $2i\pi$ phase difference between the two sinusoidal terms within the second part of $Q_N(V, t)$. This means that the two parts of the residual free vibration induced by a single moving load are canceled out.

The conditions in terms of load speed V_{canI}(km/h) for the first type of cancellation can be further derived from Eq. (2.99a, 2.99b) as

$$V_{canI} = \frac{7.2 f_n L}{2i-1}, \quad (n=1,3,5,\cdots; \quad i=1,2,3,\cdots; \quad \text{and } n \neq 2i-1) \tag{2.100a}$$

$$V_{canI} = \frac{7.2 f_n L}{2i}, \quad (n=2,\ 4,\ 6,\cdots; \quad i=1,\ 2,\ 3,\ldots; \quad \text{and } n \neq 2i) \tag{2.100b}$$

Note that the restriction conditions $n \neq 2i-1$, (n = 1, 3, 5,…) and $n \neq 2i$ (n = 2, 4, 6,…) are given in Eq. (2.100a, 2.100b), because under these values β_n becomes 1 and the second resonance condition is satisfied, which is beyond the assumption of Eq. (2.88). The speed from Eq. (2.100a, 2.100b) coincides with the cancellation speed $\alpha = n^2/k$ in Sect. 2.1.

It can be found from Eq. (2.100a, 2.100b) that the cancellation effect takes place when the force travels on the bridge at a certain speed. This type of cancellation is induced by each individual load and is independent of the number and composition of load series. The cancellation speed is related to the order of vibration mode. Because the fundamental mode provides the largest contribution to the mid-span displacement of a simply-supported bridge, it seems feasible to use Eq. (2.100a) with n = 1 to predict the cancellation speed. This is also assumed in the subsequent section.

2.4.2 *Resonance and Cancellation of Simply-Supported Beam Under a Series of Train Loads*

2.4.2.1 Analysis Model Considering Train Load Series

For a real train composed of several cars, as mentioned previously, there exist different geometric intervals: the full length l_v of the car, the rated axle distance l_c between bogie centers of a car, and the wheelbase l_w between the two wheel-sets of a bogie. Thus, an analysis model shown in Fig. 2.23 is adopted to study the influence of these intervals on the resonance and cancellation effects of a simply-supported bridge.

In this model, the loads of a train composed of N_v cars with four axles are represented by $4N_v$ moving concentrated forces expressed as P_{kj} (k = 1, 2, 3,…,N_v; j = 1, 2, 3, 4), where subscript k indicates the car number of the train and j indicates the axle number of each car. Thus, the train is modeled as groups of four moving

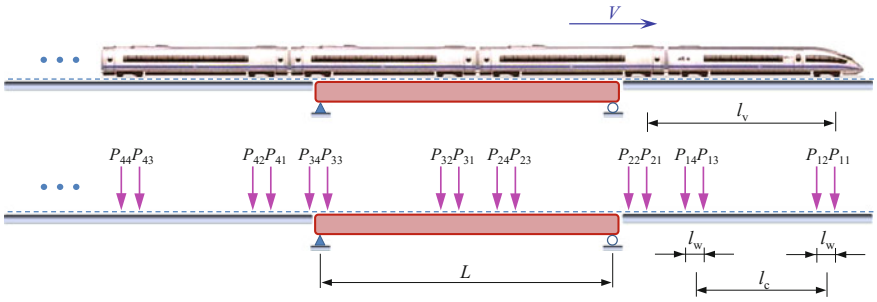

Fig. 2.23 Analysis model of train load series

concentrated forces P_{k1}, P_{k2}, P_{k3}, and P_{k4} with an identical interval l_v between similar forces of each group.

Owing to the time delays between load groups P_{k2}, P_{k3}, P_{k4}, and P_{k1}, the time for the kth force in group j traveling on the bridge can be defined as

$$\begin{cases} t_{k1}=t_k \\ t_{k2}=t_k+l_w/V \\ t_{k3}=t_k+l_c/V \\ t_{k4}=t_k+(l_c+l_w)/V \end{cases} \tag{2.101}$$

Note that $t_k = (k-1)l_v/V$ is still valid herein.

In this case, the motion equation for the bridge can be written as

$$\bar{m}\frac{\partial^2 y(x,t)}{\partial t^2}+EI\frac{\partial^4 y(x,t)}{\partial x^4}=\sum_{k=1}^{N_v}\sum_{j=1}^{4}P\delta\left[x-V(t-t_{kj})\right] \tag{2.102}$$

Considering the case when the first $(N-1)$ cars have left the bridge and only the Nth car is traveling on the bridge, the solution of Eq. (2.102) can be given directly referring to the previous analysis in Sect. 2.4.1 as

$$y(x,t)=\frac{2P}{\bar{m}L}\sum_{n=1}^{\infty}\sin\left(\frac{n\pi x}{L}\right)\frac{1}{\omega_n^2(1-\beta_n^2)}\sum_{j=1}^{4}Q_{Nj}(V,t) \tag{2.103}$$

where

$$\sum_{j=1}^{4}Q_{Nj}(V,t)=\sum_{j=1}^{4}\left[\sin\bar{\omega}_n(t-t_{Nj})-\beta_n\sin\omega_n(t-t_{Nj})\right] -2\beta_n\sum_{k=1}^{N-1}\sum_{j=1}^{4}\cos\frac{\omega_n L}{2V}\left[\sin\omega_n\left(t-t_{kj}-\frac{L}{2V}\right)\right] \quad (n=1,3,5,\ldots) \tag{2.104a}$$

$$\sum_{j=1}^{4}Q_{Nj}(V,t)=\sum_{j=1}^{4}\left[\sin\bar{\omega}_n(t-t_{Nj})-\beta_n\sin\omega_n(t-t_{Nj})\right] -2\beta_n\sum_{k=1}^{N-1}\sum_{j=1}^{4}\sin\frac{\omega_n L}{2V}\left[\cos\omega_n\left(t-t_{kj}-\frac{L}{2V}\right)\right] \quad (n=2,4,6,\ldots) \tag{2.104b}$$

By applying trigonometric transformation formulas $\sin A+\sin B=2\cos\frac{A+B}{2}\sin\frac{A-B}{2}$ and $\cos A+\cos B=2\cos\frac{A+B}{2}\cos\frac{A-B}{2}$ to the second term of the

right side of Eq. (2.104a, 2.104b), the following expressions can be obtained after rearrangement as

$$\sum_{j=1}^{4} Q_{Nj}(V,t) = \sum_{j=1}^{4} \left[\sin \bar{\omega}_n(t-t_{Nj}) - \beta_n \sin \omega_n(t-t_{Nj})\right] - 8\beta_n \cos\frac{\omega_n L}{2V}\cos\frac{\omega_n l_w}{2V}\cos\frac{\omega_n l_c}{2V} \times \sum_{k=1}^{N-1}\left[\sin\omega_n\left(t-t_{k1}-\frac{L}{2V}-\frac{l_w}{2V}-\frac{l_c}{2V}\right)\right] \quad (n=1,3,5,\ldots) \tag{2.105a}$$

$$\sum_{j=1}^{4} Q_{Nj}(V,t) = \sum_{j=1}^{4} \left[\sin \bar{\omega}_n(t-t_{Nj}) - \beta_n \sin \omega_n(t-t_{Nj})\right] - 8\beta_n \sin\frac{\omega_n L}{2V}\cos\frac{\omega_n l_w}{2V}\cos\frac{\omega_n l_c}{2V} \times \sum_{k=1}^{N-1}\left[\cos\omega_n\left(t-t_{k1}-\frac{L}{2V}-\frac{l_w}{2V}-\frac{l_c}{2V}\right)\right] \quad (n=2,4,6,\ldots) \tag{2.105b}$$

By again introducing Eq. (2.70), the above equations can be further rewritten as

$$\sum_{j=1}^{4} Q_{Nj}(V,t) = \sum_{j=1}^{4} \left[\sin \bar{\omega}_n(t-t_{Nj}) - \beta_n \sin \omega_n(t-t_{Nj})\right] - 8\beta_n \cos\frac{\omega_n L}{2V}\cos\frac{\omega_n l_w}{2V}\cos\frac{\omega_n l_c}{2V} \times \left\{\sin\omega_n\left(t-\frac{L}{2V}-\frac{l_w}{2V}-\frac{l_c}{2V}-\frac{t_{N-1}}{2}\right)\frac{\sin(N-1)\frac{\omega_n l_v}{2V}}{\sin\frac{\omega_n l_v}{2V}}\right\} \quad (n=1,3,5,\ldots) \tag{2.106a}$$

$$\sum_{j=1}^{4} Q_{Nj}(V,t) = \sum_{j=1}^{4} \left[\sin \bar{\omega}_n(t-t_{Nj}) - \beta_n \sin \omega_n(t-t_{Nj})\right] - 8\beta_n \sin\frac{\omega_n L}{2V}\cos\frac{\omega_n l_w}{2V}\cos\frac{\omega_n l_c}{2V} \times \left\{\cos\omega_n\left(t-\frac{L}{2V}-\frac{l_w}{2V}-\frac{l_c}{2V}-\frac{t_{N-1}}{2}\right)\frac{\sin(N-1)\frac{\omega_n l_v}{2V}}{\sin\frac{\omega_n l_v}{2V}}\right\} \quad (n=2,4,6,\ldots) \tag{2.106b}$$

2.4.2.2 Resonance and Cancellation Induced by a Train Load Series

The resonant conditions derived from Eq. (2.106a, 2.106b) are not different from Eq. (2.97) in Sect. 2.3. Obviously, two more cancellation conditions can be extracted from Eq. (2.106a, 2.106b) as

$$\cos(\omega_n l_w/2V) = 0 \tag{2.107a}$$

$$\cos(\omega_n l_c/2V) = 0 \tag{2.107b}$$

The corresponding cancellation train speeds V_{canII}(km/h) can be expressed as

$$V_{\text{canII}} = \frac{7.2 f_n l_{\text{w}}}{2i-1}, \quad (i = 1, 2, 3, \cdots) \tag{2.108a}$$

$$V_{\text{canII}} = \frac{7.2 f_n l_{\text{c}}}{2i-1}, \quad (i = 1, 2, 3, \cdots) \tag{2.108b}$$

The cancellation effect will be expected if conditions associated with the wheelbase l_{w} and the axle distance l_{c} between the bogie centers in Eq. (2.108a, 2.108b) are met. However, the mechanism herein is different from that described in previous section, because in this case, the cancellation occurs due to the offset of free vibrations of the bridge induced by the moving loads of different groups. Equation (2.107a) indicates that the free vibrations induced by the two axle loads of one bogie cancel each other out, while Eq. (2.107b) indicates that the free vibrations induced by the two axle loads spaced l_{v} apart cancel each other out. As a result, the residual free vibrations of the bridge become null after the first car leaves the bridge. This type of cancellation is determined by load intervals.

A more general formula can be obtained through extension of the cancellation conditions of Eq. (2.107a, 2.107b), and the corresponding cancellation train speed can be expressed as

$$V_{\text{canII}} = \frac{7.2 f_n L_{\text{ch}}}{2i-1}, \quad (i = 1, 2, 3, \cdots). \tag{2.109}$$

where L_{ch} is the characteristic interval of the load series.

This cancellation effect is herein defined as ***the second cancellation effect of vibration***. For a railway train with two bogies and four axles, the characteristic interval may be l_{c} or l_{w}. In fact, L_{ch} can be any regular interval between the axle loads in the load series; hence, l_{v} is included as well, as shown in Fig. 2.23.

Thus far, two types of cancellation effects and their conditions have been proposed, as expressed in Eqs. (2.100a, 2.100b) and (2.109), respectively. When only the fundamental mode of the bridge is concerned, the cancellation speed equation can be written in a unified form as function of the bridge span L

$$V_{\text{can}} = \frac{7.2 \alpha f_1 L}{2i-1}, \quad (i = 1, 2, 3, \cdots) \tag{2.110}$$

where f_1 is the fundamental frequency of the bridge; α is the dimensionless length parameter, which may take the value of 1 or L_{ch}/L, indicating the first or second type of cancellation, respectively.

2.4.2.3 Resonance Disappearance

The second term of Eq. (2.106a, 2.106b) will be null once cancellation conditions are satisfied even with the resonant condition synchronously met. Therefore, cancellation plays a more dominant role, and resonance disappearance may be expected when a train speed coincides simultaneously with the conditions of resonance and cancellation. When $V_{can} = V_{res}$, namely combining Eqs. (2.97) and (2.110), a new mathematical expression is obtained as

$$\frac{l_v}{L} = \frac{2\alpha k}{2j-1}, \quad (j,k = 1,2,3,\cdots) \tag{2.111}$$

where j and k are, respectively, the resonance and cancellation order for the first bending mode of the bridge. In theory, when the ratio of car length l_v to span L meets the conditions of Eq. (2.111), both the cancellation and resonance conditions may simultaneously appear at certain train speeds, and the resonance of the bridge at its fundamental mode will be avoided. Therefore, this interesting phenomenon is named as ***resonance disappearance***.

2.4.3 Numerical Verification

To verify the theoretical expressions, by using the FEM, a computation program is developed to analyze the vibration response of a single span simply-supported bridge under moving train loads.

The bridge has a span of 31.1 m, a uniform mass density of 19.1 Mg/m, and a uniform cross-sectional bending stiffness of $EI = 1.66 \times 10^8$ kN·m^2, and the first natural frequency is calculated by $f_1 = \frac{\pi}{2L^2}\sqrt{\frac{EI}{m}}$ as 4.79 Hz.

A high-speed train composed of four cars is adopted for analysis, simplified as 16 concentrated forces. The forces take the axle loads of the ICE3 high-speed train, which are 160 kN for the first and the last motor-cars ($P_1 \sim P_4$, $P_{13} \sim P_{16}$) and 146 kN for the intermediate trailer cars ($P_5 \sim P_8$, $P_9 \sim P_{12}$), respectively, as shown in Fig. 2.24.

According to the train axle intervals and the bridge span shown in Fig. 2.24, the characteristic interval L_{ch} of the load series can be $l_v = 24.775$ m, $l_c = 17.375$ m, and $l_w = 2.5$ m, and thus, the dimensionless length parameter α in Eq. (2.110) can be identified as 1.0 for the first cancellation condition, and as $l_w/L = 0.08$, $l_c/L = 0.56$, and $l_v/L = 0.79$ for the second cancellation condition. On the basis of these parameters, the resonance and cancellation speeds V_{res} and V_{can} corresponding to the fundamental mode of the bridge are calculated by Eqs. (2.97) and (2.110), and the results of the first eight orders are listed in Table 2.2.

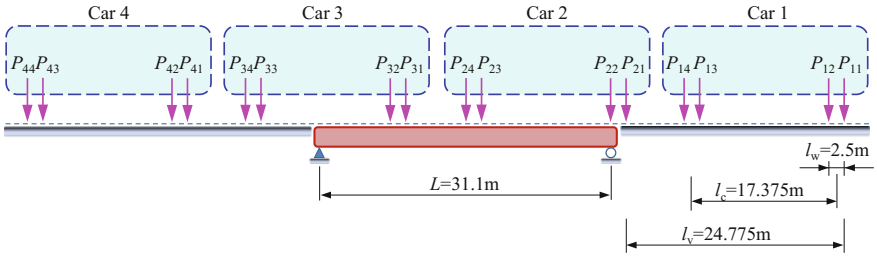

Fig. 2.24 Simply-supported bridge subjected to a moving train load series

Table 2.2 Resonance and cancellation train speeds for the 31.1 m span simply-supported bridge

Order i		1	2	3	4	5	6	7	8
Resonance train speed V_{res} (km/h)		427	214	142	107	85	71	61	–
Cancellation train speed V_{can} (km/h)	α = 1.00	N/A	358	215	153	119	98	83	72
	α = 0.08	86	–	–	–	–	–	–	–
	α = 0.56	601	200	120	86	67	–	–	–
	α = 0.79	847	282	169	121	94	77	65	–

Note "–" indicates the speeds lower than 60 km/h, which are not listed in this table

2.4.3.1 Time History Analyses of the Bridge Under Resonance and Cancellation Conditions

Resonance effect

It is known that a resonance may appear when a certain relationship is satisfied among the load moving speed, load interval, and bridge natural frequency. Herein, the first-order resonance speed 427 km/h is taken as an example to illustrate how the ICE3 train load series induces the resonance of the bridge.

Because the ICE3 load series is composed of several different intervals, the analysis is conducted in two stages, as shown in Fig. 2.25.

In the first stage, a group of loads composed of the first axle loads (P_{11}, P_{21}, P_{31}, and P_{41}) of the four cars is considered. The time delay between any two successive loads is determined by load interval l_v and resonant speed V_{res}, which can be calculated as

$$t_{res} = \frac{l_v}{V_{res}} = \frac{il_v}{f_n l_v} = iT_{bn}, \quad (i = 1, 2, 3, \cdots) \tag{2.112}$$

When only the first mode of the bridge is considered, and for the resonant speed related to $i = 1$, the time delay is equal to the bridge natural period T_b, thus producing a 2π phase difference between the free vibrations of the bridge induced by any two successive loads in this group. In this case, the amplitudes of the bridge in

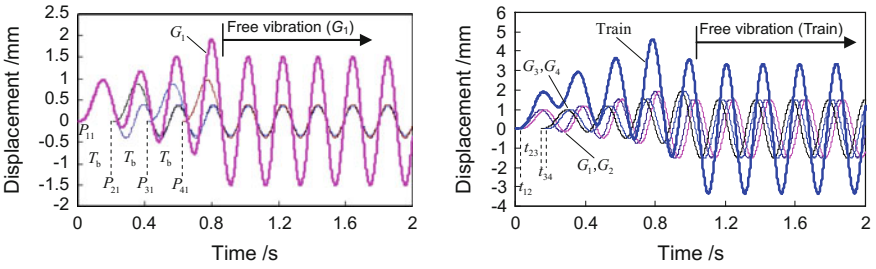

(a) Induced by equidistance loads (b) Superposition of various loads

Fig. 2.25 Displacement histories of the bridge at mid-span under V_{res} = 427 km/h

the free vibration stage will be directly superposed to form a resonant displacement curve G_1, as shown in Fig. 2.25a.

Similarly, the resonant displacement curve G_2 induced by the load series composed of the second axle loads (P_{12}, P_{22}, P_{32}, and P_{42}) of the four cars can be obtained and so for G_3 and G_4.

In the second stage, the four resonant displacement curves ($G_1 \sim G_4$) induced by the four groups of load series are superposed together according to the time delays determined by their intervals l_w, l_c, and $l_w + l_c$. Thus, the bridge displacement induced by the whole train can be obtained, as shown in Fig. 2.25b.

It is easy to see that under the resonant speed, the displacement of the bridge will be successively amplified with an increasing number of loads, which explains the physical meaning of Eq. (2.96a, 2.96b).

The first cancellation effect

Parameter $\alpha = 1$ corresponds to the first type of cancellation. The third-order ($\alpha = 1$, $i = 3$) cancellation speed 215 km/h in Table 2.2 is selected as an example to illustrate how the first cancellation effect appears. Shown in Fig. 2.26 are the calculated displacement histories of the bridge induced by the train (four cars), the first car, and its four individual axle loads $P_{11} \sim P_{14}$.

The mechanism for the first type of cancellation can be observed clearly in these displacement histories. It is found that each moving load induces a forced vibration

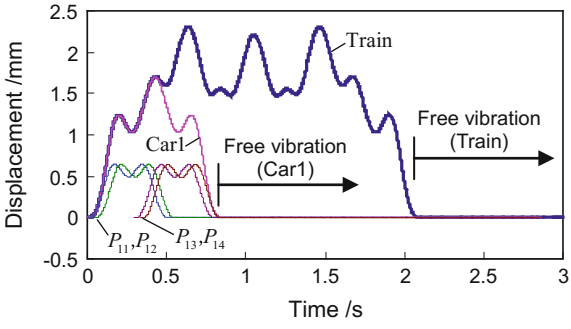

Fig. 2.26 Displacement histories of the bridge induced by the train, Car 1, and its four individual loads ($P_{11} \sim P_{14}$) under V_{can1} = 215 km/h

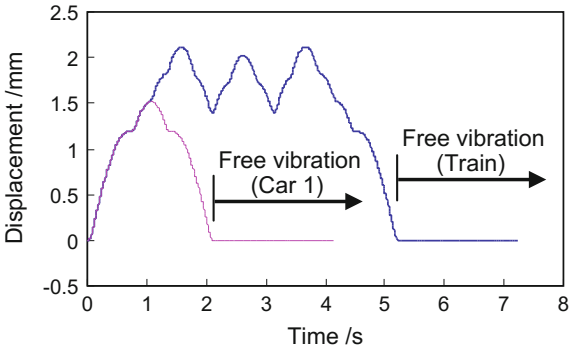

Fig. 2.27 Displacement histories of the bridge induced by the train and Car 1 under V_{canII} = 86 km/h

of the bridge, but when it leaves, the free vibration of the bridge is null. As a result, the free vibration of the bridge remains zero when the first car as well as the train leaves the bridge. This numerical example explains the physical meaning of Eq. (2.100a, 2.100b).

The second cancellation effect

In Table 2.2, $\alpha = 0.08$ and $\alpha = 0.56$ correspond to the second type of cancellation speeds, which are derived from wheelbase l_w of a bogie and axle distance l_c between the bogie centers of a car, respectively.

Obviously, $V_{canII} = 86$ km/h is the most opportune cancellation speed for comparison, for it appears twice in the table at $\alpha = 0.08$ ($i = 1$) and $\alpha = 0.56$ ($i = 4$), respectively, so it is selected as an example to illustrate the effect of the second cancellation. The mechanism of this type of cancellation is clearly illustrated in Fig. 2.27, which gives the displacement histories of the bridge at mid-span induced by the train and the first car only.

It is seen that at this cancellation speed no free vibration of the bridge appears when the first car as well as the train leaves the bridge, because the cancellation speed $V_{canII} = 86$ km/h is the first-order cancellation speed ($\alpha = 0.08$) related to l_w and also the fourth-order cancellation speed ($\alpha = 0.56$) related to L_c. When $\alpha = 0.08$ and $i = 1$, the free vibrations induced by P_{11} and P_{12} cancel each other out, same for P_{13} and P_{14}. When $\alpha = 0.56$ and $i = 4$, the free vibrations induced by P_{11} and P_{13} cancel each other out and also P_{12} and P_{14}. As a result, no free vibration remains when each car leaves the bridge, and the displacement of the bridge is determined only by the loads still on it.

The mechanism of the second type of vibration cancellation is further explained in Fig. 2.28. At $V_{can} = 86$ km/h, the cancellation effect appears between the two axle loads separated by l_w or l_c.

Figure 2.28a illustrates the mechanism of the second cancellation effect corresponding to P_{11} and P_{12} with a wheelbase l_w. It can be found that the displacement of the bridge induced by P_{12} has a time delay of $T_b/2$ related to P_{11}, producing a phase difference π between them and causing the free vibrations by P_{11} and P_{12} having the same amplitudes but opposite phases. The result is null vibration when this pair of loads leaves the bridge.

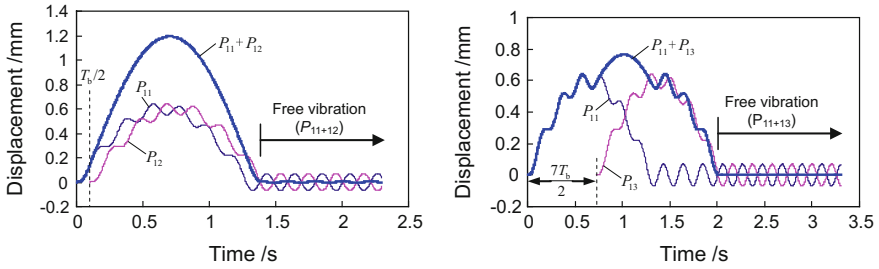

(a) V_{can}=86 km/h, l_w=2.5 m, i=1 (b) V_{can}=86 km/h, l_c=17.375 m, i=4

Fig. 2.28 Displacement histories of the bridge under V_{canI} = 86 km/h

Figure 2.28b shows the mechanism of the second cancellation effect corresponding to P_{11} and P_{13} with an interval l_c. In this case, the time delay between P_{13} and P_{11} becomes 7 T_b/2, and the phase difference becomes 7π; thus, the free vibrations induced by the two loads cancel each other out. Similar cancellation effects exist between the other pairs of loads (P_{12} + P_{14}).

The time delay between the two loads can be calculated by the interdistance and cancellation speed of the loads as follows:

$$t_{can} = \frac{L_{ch}}{V_{can}} = \frac{(2i-1)L_{ch}}{2f_n L_{ch}} = \frac{(2i-1)}{2} T_{bn}, \quad (i = 1, 2, 3, \ldots) \tag{2.113}$$

When only the first mode of the bridge is considered, it is calculated from Eq. (2.113) that at V_{canII} = 86 km/h, the time delays for the two pairs of loads are T_b/2 (i = 1) and 7 T_b/2 (i = 4), respectively, as marked in Fig. 2.28, and thus, the displacements of the bridge induced by them completely cancel out.

2.4.3.2 Relationship Between Resonance and Cancellation Effects

It was mentioned previously that the condition of cancellation is more dominant over that of resonance. Therefore, cancellation plays a more dominant role and resonance disappearance may be expected when the train speeds coincide with both conditions of resonance and cancellation. In the subsequent section, the relationship between resonance and cancellation effects is discussed.

Suppression of resonance by the first cancellation effect

It is interesting to notice from Table 2.2 that the cancellation speed V_{canI} = 215 km/h is very close to the resonance speed V_{res} = 214 km/h (i = 2), which means this resonant speed approximately meets the cancellation condition. To better describe what will happen, the time histories of bridge mid-span displacements induced by a single load P_{11}, the first car, and the whole train under V_{res} = 214 km/h are calculated, as shown in Fig. 2.29a.

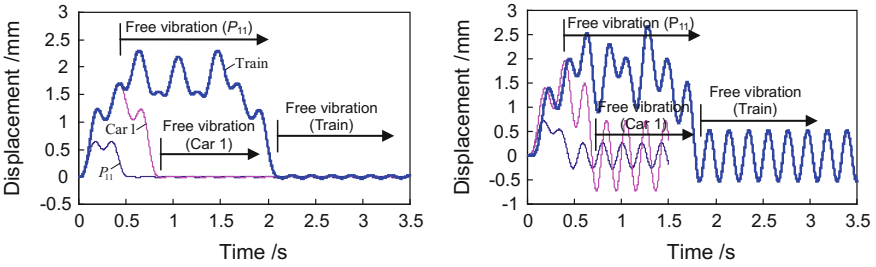

(a) V_{res}=214 km/h (b) V=250 km/h

Fig. 2.29 Displacement histories of the bridge induced by single load P_{11}, Car 1, and train

The resonant speed determined by Eq. (2.97) corresponds to the resonance effect that is provoked by the successive amplification of the bridge displacement with an increasing number of loads on the bridge. As shown in Fig. 2.29a, because the speed 214 km/h is very close to the first type of cancellation speed V_{canI} = 215 km/h, the free vibration of the bridge induced by each individual load is approximately equal to zero, and thus, the bridge displacement induced by a series of loads after superposition of all effects of them is also very small. Therefore, when the resonant speed is close to the cancellation speed, the resonance effect is suppressed by the cancellation effect, resulting in small bridge vibrations.

For comparison, the time histories of the bridge displacement at the train speed of 250 km/h, which is neither a resonance speed nor a cancellation one, are shown in Fig. 2.29b. It is clear that neither the free vibrations induced by the first axle load nor by the car 1 is zero. Hence, after the whole train leaves the bridge, there remains a high residual response (free vibration) on the bridge.

Suppression of resonance by the second cancellation effect

According to Table 2.2, the cancellation speed V_{canII} = 86 km/h is very close to the resonance speed V_{res} = 85 km/h (i = 5). To better describe what will happen in this situation, the time histories of bridge displacements induced by two loads, P_{11} and P_{21}, are calculated, as shown in Fig. 2.30a.

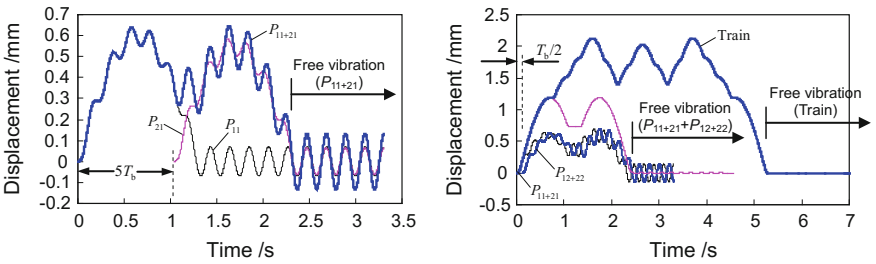

(a) Resonance effect (V_{res}=85 km/h, i=5) (b) Resonance suppression (V_{can} =86 km/h, i=4)

Fig. 2.30 Displacement histories of the bridge at mid-span

Using Eq. (2.112), it is calculated that under 85 km/h, the time delay between the two loads P_{11} and P_{21} is 5 T_b (i = 5). In this case, the phase gap between free vibrations induced by P_{11} and P_{21} is 10π, which indicates five vibration periods, and thus, the free vibrations induced by the two loads superpose each other.

However, in this special case, because the resonant speed 85 km/h is very close to the cancellation speed 86 km/h, the resonance will be suppressed. The mechanism of resonance suppression is shown in Fig. 2.30b, where P_{11} and P_{21} reflect the resonance effect of P_{11+21}, and P_{12} and P_{22} reflect the resonance effect of P_{12+22}. Because the time delay between P_{11+21} and P_{12+22} at 85 km/h is quite close to T_b/2, the resultant free vibrations of the bridge subjected to these two pairs of loads almost cancel each other out. When the whole train leaves the bridge, the free vibration remains very small.

Influence of cancellation effect on resonance

To further investigate the relationship between the derived theoretical resonance and cancellation conditions, a numerical analysis is carried out for the dynamic responses of the bridge subjected to the train load series shown in Fig. 2.24, within the speed range of 70 ∼ 500 km/h.

Shown in Fig. 2.31 is the distribution of the calculated DAF (Dynamic Amplification Factor) of the bridge mid-span deflection versus train speed.

It is observed that the DAF does not increase monotonously with the train speed, while there appear several peaks at particular train speeds. When the resonance and cancellation speeds listed in Table 2.2 are marked on the DAF curve, the influence of resonance and cancellation conditions can be clearly observed.

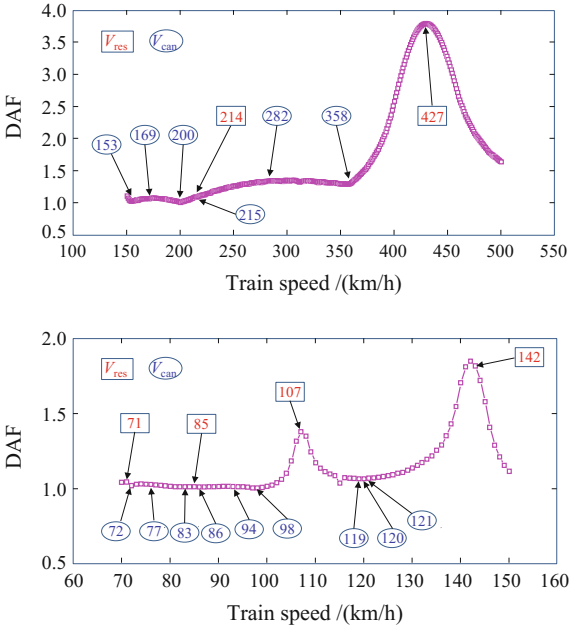

Fig. 2.31 Distribution curves of bridge deflection DAF versus train speed

Obvious peaks on the DAF curves appear at the resonance train speeds 427, 142, and 107 km/h, indicating the resonance phenomena indeed happen at these speeds.

At the resonance speeds of 214, 85, and 71 km/h, however, similar cancellation speeds of 215, 86, and 72 km/h exist, resulting in relatively small DAF values. This numerically proves that when a load series speed simultaneously meets both the resonance and cancellation conditions, the cancellation effect plays a dominant role and the resonance effect will be suppressed; namely, a resonance disappearance occurs. Hence, when the ratio of car length l_v to bridge span L meets the conditions of Eq. (2.111), there will be $V_{res} = V_{can}$ at certain speeds, which provides the possibility of eliminating the resonance. For the considered 31.1 m span simply-supported bridge and the ICE3 train, if the resonance at speed 214 km/h is counteracted, the dynamic responses of the bridge will remain at a low level in the whole speed range of 150 $\sim$ 350 km/h, which is of practical significance in bridge design and the running safety of high-speed trains.

2.4.3.3 Influence of Damping on the Cancellation Effect

In the previous theoretical and numerical analyses, the influence of damping was ignored. In reality, the free vibration of a bridge will attenuate gradually because of the existence of damping. Thus, in the second cancellation effect, the free vibrations induced by a pair of loads will not completely cancel each other out, even if they have the same amplitude and opposite phases. To illustrate the influence of damping on the second type of cancellation, the cancellation speed of 86 km/h is taken again as an example, which corresponds to $\alpha = 0.08$ ($i = 1$) and $\alpha = 0.56$ ($i = 4$). A damping ratio of 0.05 is used to calculate the displacement of the bridge subjected to two loads, as shown in Fig. 2.32.

It can be found that the existence of damping only changes the amplitudes of the free vibration of the bridge, while it affects little the vibration period because the difference between damped and undamped periods is very small. Thus, under the cancellation speed of 86 km/h, the time delay between P_{11} and P_{12} is $T_b/2$ ($i = 1$)

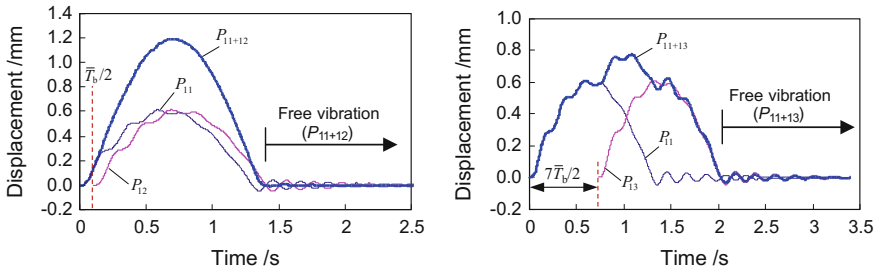

(a) V_{can}=86km/h, L_w=2.5m, i=1 (b) V_{can}=86km/h, L_c=17.375m, i=4

Fig. 2.32 Displacement histories of the bridge considering damping ratio 0.05 under V_{can} = 86 km/h

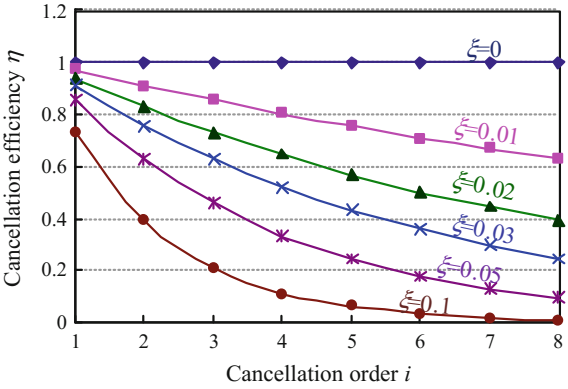

Fig. 2.33 Distributions of cancellation efficiency versus cancellation order for different damping ratios

and that between P_{11} and P_{13} is $7T_b/2$ ($i = 4$), which are approximately equal to those in the undamped case. However, the displacements of free vibration induced by the two loads cannot perfectly cancel each other out despite their opposite phases. This is because they have different absolute values as a result of the unequal time of damping attenuations. It can be concluded that the time delay between the two loads affects the canceling extent of the bridge free vibration, and obviously, the longer the time delay, the less the free vibration can be canceled, thus lowering the cancellation effect.

Of course, the value of damping has a direct influence on the cancellation effect. Figure 2.33 illustrates the distribution of the cancellation efficiency η (defined as the ratio of the maximum free vibration displacement of the bridge that has been canceled out to the one without cancellation) with respect to the cancellation order under several different damping ratios. It can be found that the higher the damping, and the longer the delay time (reflected by the cancellation order) between the two loads, the lower is the cancellation efficiency. Despite this, the cancellation efficiency η is greater than 0.5 for the first two cancellation orders with the bridge damping ratio in the range of $0 \sim 0.05$.

2.4.3.4 Conclusions

The mechanisms of vibration resonance and cancellation for a simply-supported bridge subjected to a moving load series are investigated theoretically and are verified through finite-element numerical simulations. The following conclusions can be drawn:

(1) A resonant vibration may occur because of the superposition of vibrations induced by a series of moving loads passing over a simply-supported bridge when the time interval between two adjacent loads equals the natural period of the bridge or its ith ($i = 1, 2, 3,\ldots$) multiples.

(2) The free vibration of the bridge induced by a single moving load may be canceled out to null by itself when the load speed satisfies a certain relationship with the span length and the natural frequencies of the bridge. This is defined as the first cancellation effect. The first cancellation condition is related to a single load behavior, while it is independent of the numbers and arrangement of loads. The critical cancellation speed expression is associated with the order n of the vibration mode.
(3) The free vibrations of the bridge induced by a series of moving loads may cancel each other out when the load speed satisfies a certain relationship with the load interval and the natural frequencies of the bridge. This is defined as the second cancellation effect, which is related to the interval between any two loads, namely the arrangement of the load series. The second cancellation condition is related to the characteristic interval of loads.
(4) The damping of the bridge has an influence on the efficiency of the second type of cancellation: The higher the damping and the longer the delay time between two loads, the lower is the cancellation efficiency.
(5) In some cases, a certain train speed may simultaneously satisfy both resonance and cancellation conditions. If this occurs, the cancellation plays a dominant role and a resonance disappearance can be expected. This provides the possibility of avoiding bridge resonance via proper design, which is of theoretical as well as practical significance in the dynamic design of high-speed railway bridges.

References

Cheung YK, Au FTK, Zheng DY, Cheng YS (1999) Vibration of multi-span bridges under moving vehicles and trains by using modified beam vibration functions [J]. J Sound Vib 228 (3):611–628

Clough RW, Penzien J (2003) Dynamics of structures [M]. McGraw Hill Inc, New York

Diana G, Cheli F (1989) Dynamic interaction of railway systems with large bridges [J]. Veh Sys Dyn 18:71–106

Frýba L (1999) Vibration of solids and structures under moving loads [M]. Thomas Telford, London

Frýba L (2001) A rough assessment of railway bridges for high speed trains [J]. Eng Struct 23 (5):548–556

Garinei A, Risitano G (2008) Vibrations of railway bridges for high-speed trains under moving loads varying in time [J]. Eng Struct 30(3):724–732

Hamidi SA, Danshjoo F (2010) Determination of impact factor for steel railway bridges considering simultaneous effects of vehicle speed and axle distance to span length ratio [J]. Eng Struct 32(5):1369–1376

Ju SH, Lin HT (2003) Resonance characteristics of high-speed trains passing simply-supported bridges [J]. J Sound Vib 267(5):1127–1141

Kwark JW, Choi ES, Kim YJ et al (2004) Dynamic behavior of two-span continuous concrete bridges under moving high-speed train [J]. Comput Struct 82(4–5):463–474

Lee HH, Jeon JC, Kyung KS (2012) Determination of a reasonable impact factor for fatigue investigation of simple steel plate girder railway bridges [J]. Eng Struct 36:316–324

Li JZ, Su MB (1999) The resonant vibration for a simply-supported girder bridge under high speed trains [J]. J Sound Vib 224(5):897–915
Liu K, Reynders E, De Roeck G, Lombaert G (2009) Experimental and numerical analysis of a composite bridge for high-speed trains. J Sound Vib 320(1–2):201–220
Luu M, Zabel V, Könke C (2012) An optimization method of multi-resonant response of high-speed train bridges using TMDs [J]. Finite Elem Anal Des 53:13–23
Lavado J, Doménech A, Martínez-Rodrigo MD (2014) Dynamic performance of existing high-speed railway bridges under resonant conditions following a retrofit with fluid viscous dampers supported on clamped auxiliary beams [J]. Eng Struct 59:355–374
Matsuura A (1976) A study of dynamic behavior of bridge girder for high speed railway [J]. Proc Jpn Civil Eng Soc 256:35–47 (in Japanese)
Michaltsos GT, Raftoyiannis IG (2010) The influence of a train's critical speed and rail discontinuity on the dynamic behavior of single-span steel bridges [J]. Eng Struct 32(2):570–579
Museros P, Moliner E, Martínez-Rodrigo MD (2013) Free vibrations of simply-supported beam bridges under moving loads: maximum resonance, cancellation and resonant vertical acceleration [J]. J Sound Vib 332(2):326–345
Pesterev AV, Yang B, Bergman LA, Tan CA (2003) Revisiting the moving force problem. J Sound Vib 261(1):75–91
Rade L, Westergren B (2010) Mathematics handbook for science and engineering. Springer
Rocha JM, Henriques AA, Calçada R (2012) Safety assessment of a short span railway bridge for high-speed traffic using simulation techniques [J]. Eng Struct 40:141–154
Savin E (2001) Dynamic amplification factor and response spectrum for the evaluation of vibrations of beams under successive moving loads [J]. J Sound Vib 248(2):267–288
TB10002.1-2005 (2005) Fundamental code for design on railway bridge and culvert [S]. China Railway Publishing House, Beijing
TJS 2003-13 (2003) Interim provisions on design of Beijing-Shanghai HSR [S]. China Railway Publishing House, Beijing (in Chinese)
TJS 2005-285 (2005a) Interim provisions on design of 200 km/h new railways for passenger and freight trains [S]. China Railway Publishing House, Beijing (in Chinese)
TJS 2005-285 (2005b) Commentary on interim provisions on design of 200 km/h new railways for passenger and freight trains [S]. China Railway Publishing House, Beijing (in Chinese)
Xia H, Chen YJ (1992) Dynamic interaction analysis of train-beam-pier system [J]. China Civil Eng J 25(2):3–12 (in Chinese)
Xia H, Zhang N (2005) Dynamic interaction of vehicles and structures [M]. Beijing Science Press (in Chinese)
Xia H, Zhang N, Guo WW (2006) Analysis of resonance mechanism and conditions of train-bridge system [J]. J Sound Vib 297(3–5):810–822
Xia H, De Roeck G, Goicolea JM (2012) Bridge vibration and controls: new research [M]. Nova Science Publishers Inc, New York
Xia H, Li HL, Guo WW, De Roeck G (2014) Vibration resonance and cancellation of simply-supported bridges under moving train loads [J]. J Eng Mech ASCE 140 (5):04014015-1-11
Yang YB, Yau JD, Hsu LC (1997) Vibration of simple beams due to trains moving at high speeds [J]. Eng Struct 19(11):936–944
Yang YB, Yau JD, Wu YS (2004a) Vehicle-bridge interaction dynamics [M]. World Scientific Publishing, Singapore
Yang YB, Lin CL, Yau JD, Chang DW (2004b) Mechanism of resonance and cancellation for train-induced vibrations on bridges with elastic bearings [J]. J Sound Vib 269(1–2):345–360
Yau JD (2001) Resonance of continuous bridges due to high speed trains [J]. J Mar Sci Technol 9 (1):14–20
Yau JD, Wu YS, Yang YB (2001) Impact response of bridges with elastic bearings to moving loads [J]. J Sound Vib 248(1):9–30

Yau JD, Yang YB (1999) Theory of vehicle-bridge interaction for high-speed railway [M]. DNE Press, Taipei

Zambrano A (2011) Determination of the critical loading conditions for bridges under crossing trains [J]. Eng Struct 33(2):320–329

http://www.springer.com/978-3-662-54869-1

Dynamic Interaction of Train-Bridge Systems in High-Speed Railways
Theory and Applications
Xia, H.; Zhang, N.; Guo, W.
2018, XVI, 580 p. 358 illus., 357 illus. in color.,
Hardcover
ISBN: 978-3-662-54869-1